WADC TECHNICAL REPORT 54-370

INTERIM REPORT ON

HUMAN FREQUENCY RESPONSE STUDIES

Ezra S. Krendel
George H. Barnes

The Franklin Institute Laboratories
for Research and Development

June 1954

Aircraft Laboratory and
Aero Medical Laboratory
Contract No. AF 33(038)-10420
E. O. No. 694-39

Wright Air Development Center
Air Research and Development Command
United States Air Force
Wright-Patterson Air Force Base, Ohio

WADC TECHNICAL REPORT 54-370

INTERIM REPORT ON HUMAN FREQUENCY RESPONSE STUDIES

EZRA S. KRENDEL
GEORGE H. BARNES
THE FRANKLIN INSTITUTE LABORATORIES
FOR RESEARCH AND DEVELOPMENT

JUNE 1954

WRIGHT AIR DEVELOPMENT CENTER

NOTICES

When Government drawings, specifications, or other data are used for any purpose other than in connection with a definitely related Government procurement operation, the United States Government thereby incurs no responsibility nor any obligation whatsoever; and the fact that the Government may have formulated, furnished, or in any way supplied the said drawings, specifications, or other data, is not to be regarded by implication or otherwise as in any manner licensing the holder or any other person or corporation, or conveying any rights or permission to manufacture, use, or sell any patented invention that may in any way be related thereto.

The information furnished herewith is made available for study upon the understanding that the Government's proprietary interests in and relating thereto shall not be impaired. It is desired that the Judge Advocate (WCJ), Wright Air Development Center, Wright-Patterson Air Force Base, Ohio, be promptly notified of any apparent conflict between the Government's proprietary interests and those of others.

FOREWORD

This report presents the background and the results of a series of experiments performed at the Franklin Institute Laboratories for Research and Development with the purpose of determining frequency response characteristics for jet pilots. This report was prepared by the Franklin Institute with Ezra S. Krendel acting as project leader under USAF Contract No. AF 33(038)-10420 covering work on Human Frequency Response. The Contract was initiated under a project identified by Research and Development Order No. R694-38-PO-6, Servo Analysis of Human Control Systems, which was sponsored jointly by the Aeromedical Laboratory and the Aircraft Laboratory, both of Wright Air Development Center. Messrs. John W. Senders and Melvin J. Warrick acted as project engineers for the Aero Medical Laboratory and Mr. Charles B. Westbrook acted as project engineer for the Aircraft Laboratory.

ABSTRACT

Linearized open loop human transfer functions or "descriptive functions" have been measured using random forcing function inputs to pilots flying an F-80A simulator. Three input bandwidths, 1, 2, and 4 radians per second and three amplitudes of 0.3, 0.6, and 1.2 rms inches were used on the display oscilloscope. Four jet pilots served as subjects. The results are phase and amplitude characteristics of the pilots for aileron and elevator control in response to visual signals displayed on a CRO.

Within the limits of the experiments performed it appears that changes in open loop "human transfer functions" because of day to day variations and different pilots are not significant. Phase characteristics were only weakly dependent on forcing function amplitude and bandwidth. The pilot's "transfer functions" for aileron and elevator control were clearly different.

Figures 11-14, in the body of this report, present a reasonable first estimate of the open loop pilot "transfer functions" used in flying an F-80A jet aircraft.

PUBLICATION REVIEW

This report has been reviewed and is approved.

FOR THE COMMANDER:

JACK BOLLERUD
Colonel, USAF (MC)
Chief, Aeromedical Laboratory
Directorate of Research

TABLE OF CONTENTS

LIST OF ILLUSTRATIONS

LIST OF ILLUSTRATIONS (continued)

INTRODUCTION

Background

This report summarizes one stage in a project whose goal is the mathematical description of control responses that are generated by a pilot while flying a high-speed airplane. The purpose of the mathematical description is to make available to aircraft designers data which may be used to improve the stability and control characteristics of piloted aircraft. This mathematical description of pilot responses consists of phase and amplitude functions of frequency which were measured experimentally in an aircraft simulator.

After some preliminary thought the following measurement program was established for the study of pilot control responses. The visual display on a cathode ray oscilloscope, which is mounted in the simulator, is to provide a two-dimensional input signal to the pilot, and the pilot's responses in controlling aileron and elevator are to be considered as providing output signals. If these signals are recorded properly we can compute the cross spectra between the input and output signals arising when the pilot flies the aircraft simulator. Measurements such as these form the basis of the experimental program.

Description of Equipment

A dynamic simulator for an F-80A, which is described in detail elsewhere, is the major experimental tool used for the measurement of pilot responses (Ref. 1, 2). This simulator contains a cockpit in which a 5 inch CRO tube presents the visual display; the display consists of a horizon and a pip representing the pilot's target (Fig. 1). The associated analog computing equipment, needed to solve the equations which make the simulator "fly like an airplane", is shown together with the cockpit and data reduction apparatus in Figure 2. In our particular experiments an F-80A flying at 20,000 feet and Mach .7 in a tail chase after a target was simulated with regard to both equations of flight and stick forces.

The inputs to the system were generated by a filtered white noise source, which made available bandwidths of 1, 2, and 4 radians per second at continuously adjustable rms voltage levels for use as forcing functions. Further details about this device may be found in Appendix I.

The data reduction in this experiment was performed by an analog computer which is shown in Figure 3. Although this device is substantially the same as described in a previous report (Ref. 3), certain changes in procedure have been made; these changes are described in Appendix II. In brief, the data reduction device accepts four signal channels which are in turn used in the computation of power spectra and cross spectra.

The execution of a series of experiments based on a theoretical approach, described in a series of working papers written on this project (Ref. 4-10), became possible with the completion of the data reduction apparatus. Because of difficulties in the operation of the data reduction apparatus experimental results were neither as decisive or plentiful as had been hoped. Approximately 120 two minute records were obtained using four jet pilots as subjects, but no more than 40% of these records were usable. Prior to running experiments with jet pilots as subjects, data were obtained using non-pilots as subjects in a series of minor experiments which were used to check out the equipment.

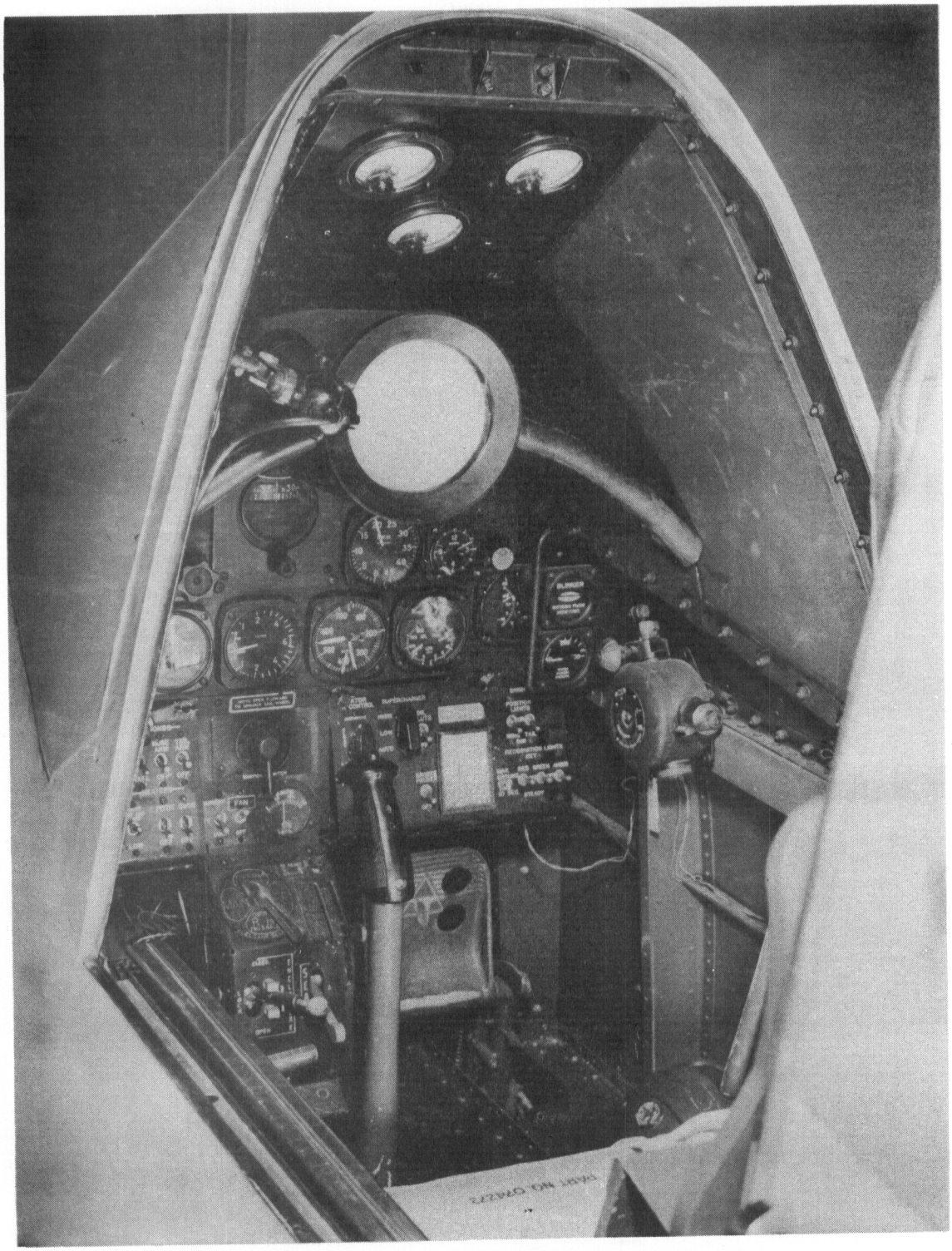

INTERIOR OF COCKPIT

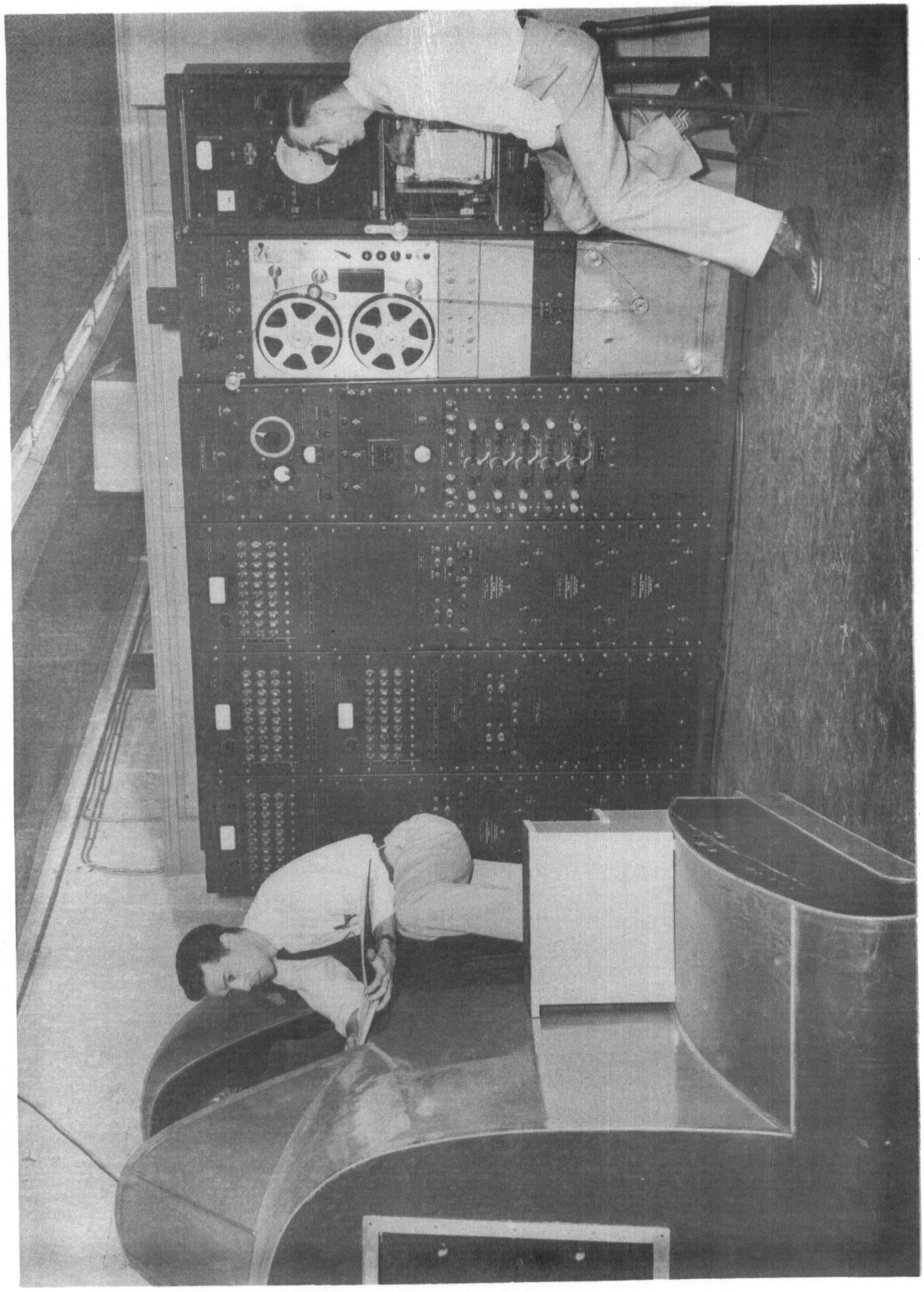

COCKPIT AND ANALOG COMPUTER RACKS

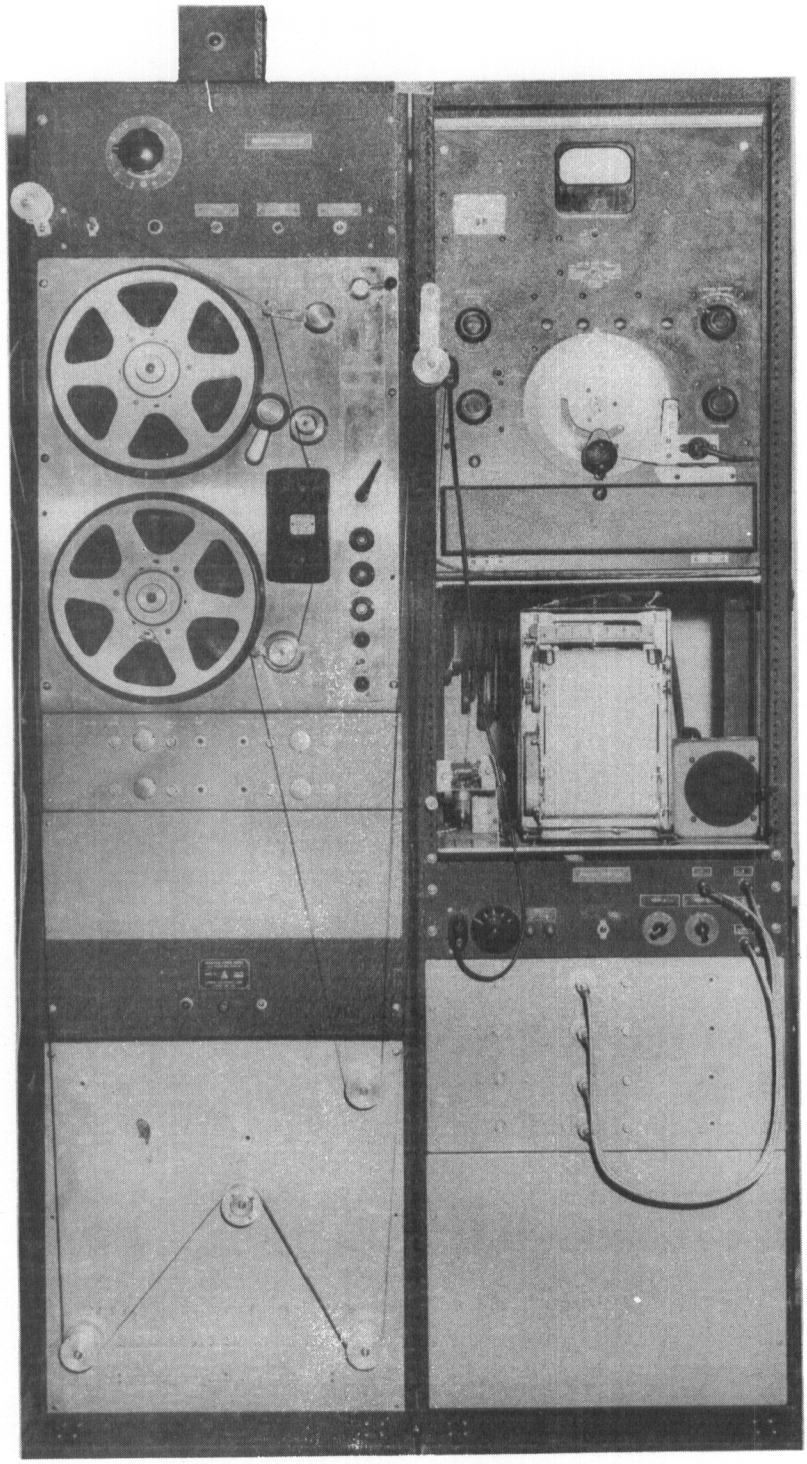

CROSS SPECTRAL DENSITY COMPUTER

I. THEORY

A. THE PROBLEM

In the problem of flying an airplane or tracking with a computing sight the human operator acts like a sensing and control device generating signals upon which either an airplane or a computer feeds. How can we characterize the process whereby the human operator transforms the signals which he senses to those signals which he presents to the apparatus under his control? In other words, we are interested in the human operator acting as a transducer. Before attempting a description of this transducer action one must think of the over-all criterion for the system of which the man is a part. It is the over-all criterion which will determine the best form for internal criteria. Since, in general, the external criterion will be closely related to some servomechanism concept such as stability or speed of response, it is reasonable to attempt to express the internal criteria in a form compatible with the demands of servomechanism analysis. Such indices of performance as time on target, probability of exceeding a given error, mean error, trials needed to attain a given level of performance, and so forth, although interesting, do not in general fit in with the demands imposed by the mathematics involved in linear servomechanism analysis. Servomechanism analysis generally deals, when possible, with frequency domain descriptions of component operation. This is to say the phase and amplitude responses as functions of frequency for the various components of the system are the quantities which are useful in calculations. As a consequence, in studying human pilot responses while the subject is flying an aircraft, one is forced to think in terms of a frequency domain analysis. By so doing, we are making the implicit assumption that a linear operator will serve to describe most of the human operator's performance. The particular manner in which a frequency domain analysis is applied is dictated by other conditions peculiar to the system under study.

B. NECESSARY MEASUREMENTS

The advisability of a frequency analysis which will be compatible with linear servo theory has been indicated. However, what sort of frequency analysis should be performed? The human operator is inherently non-linear and as such conventional techniques for servoanalysis are not applicable (Ref. 11). On the other hand the complexity of non-linear techniques is such as to make their application undesirable.

A compromise of sorts may be achieved by pursuing an argument such as the following. The drawback in solutions to non-linear equations is that a large family of particular solutions is needed to provide a general solution to the equations. Linear equations, by dint of the fact that we know they are linear, allow us to obtain the general solution quite simply. One proper measurement within the linear range serves to characterize a general solution to a linear system. Since we can't generalize from a priori system information when attempting to characterize human operators, we must seek other means for generalization short of turning to the technique of computing a host of particular solutions. One could generalize by manipulating the input signal so as to create an input which was typical of a large class of inputs which the device would encounter in practice. Thus, a time-stable response to this input might be considered to be the average response, in a sense, to a family of inputs. The mathematical operator which describes this human transducer action in converting a "typical" visual input to a typical control response output might be called, by a loose analogy to a transfer function, a "descriptive function". The "descriptive function" is the transfer function in the linearized man-machine system. It might be mentioned that for linear systems the techniques which determine the "descriptive function" will, of course, determine the transfer function. These techniques are not limited to the study of human operators, but are useful for characterizing any linearized or pseudo linear device.

In previous reports (Ref. 12-14) a preliminary attempt was made to implement the foregoing notions. Those reports made use of the fact that for a linear device the magnitude of the closed loop transfer function, $H'(\omega)$, is equal to the square root of the ratio of the power spectrum of the output signal, $\bar{\Phi}_{oo}(\omega)$, to the power spectrum of the input signal, $\bar{\Phi}_{ii}(\omega)$.

$$|H'(\omega)| = \sqrt{\frac{\bar{\Phi}_{oo}(\omega)}{\bar{\Phi}_{ii}(\omega)}} \qquad (1)$$

The results of the report were not conclusive, and the computations were inadequate since $|H'(\omega)|$ was computed instead of $H'(\omega)$. For a linear device

$$H'(\omega) = \frac{\bar{\Phi}_{io}(\omega)}{\bar{\Phi}_{ii}(\omega)} \qquad (2)$$

Where, in equation (2), $\bar{\Phi}_{io}(\omega)$ is the cross spectrum between the input and the output signal. This expression, which bears phase information, and which allows the computation of a signal to noise ratio, is much more valuable than $|H'(\omega)|$. The reason why $|H'(\omega)|$ was computed in References 12-14 is that it was half the effort to compute power spectra as it was to compute cross spectra, since the power spectrum is real and the cross spectrum is a complex function. This drawback, trivial as it

is, was the deciding factor in limiting the computations to power spectra along. As a consequence any noise which the human operator injected into the output was undetectable. Nevertheless, the idea in References 12-14 was that a suitably selected spectrum for the visual input signal would permit the calculation of a linear equivalent pseudo transfer function or "descriptive function".

In the work which the present report describes, cross spectra were computed and a filtered white noise was provided for the input function. Figure 4 illustrates the aircraft simulator problem.

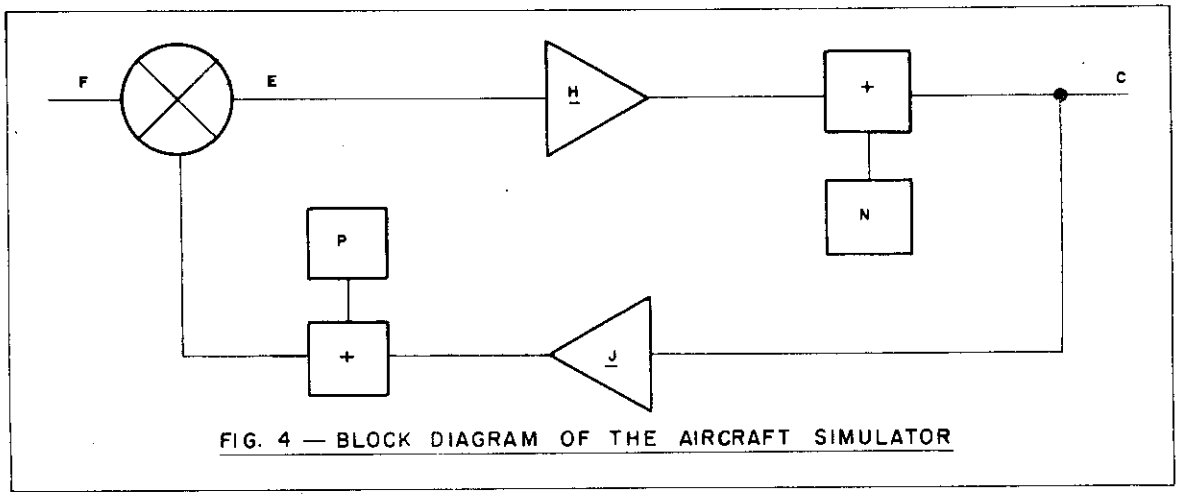

FIG. 4 — BLOCK DIAGRAM OF THE AIRCRAFT SIMULATOR

The following notation will be used in Figure 4 and throughout the rest of this report. All but H( ) and J( ) are Fourier transforms.

SYMBOLS	DEFINITIONS
$F \equiv F(\omega)$	The spectrum of the forcing function presented to the pilot-airplane system. F is generated by the noise source discussed in Appendix I.
$E \equiv E(\omega)$	The error signal visually presented on the oscilloscope face.
$C \equiv C(\omega)$	The control response made by the pilot in response to $E(\omega)$.
$\underline{H} \equiv H(\omega)$	The open loop "transfer function" describing the pilot's input-output transformation.
$N \equiv N(\omega)$	The noise which the pilot injects into his output which is uncorrelated with F.

$P = P(\omega)$	Aircraft simulator noise which is generated unintentionally. This is <u>not</u> correlated with the noise intentionally generated for F.
$\underline{J} = J(\omega)$	The airplane's transfer function.

It was decided that the forcing function, F, which would best serve to permit generalization of results by means of a generalized stimulus, was a random function whose spectrum was very similar to the spectra of a large class of practical input functions. Note that this function, with a Gaussian amplitude distribution, provides a built-in technique for getting an average response to a family of input amplitudes. Although the bandwidths of the low pass filter, which filtered the white noise source to provide the forcing function, were chosen to suit the problem of tracking a target through turbulent air, the accuracy with which turbulence is simulated is not critical. One could boldly assume that corner frequencies of 1, 2, and 4 cps present an adequate spectral range to describe pilot control responses under flight conditions. Selecting a filtered white noise makes it impossible for the pilot to engage in long term prediction. The existence of derivatives in the signal does, however, allow a small amount of short time pilot prediction.

By referring to the block diagram of the problem and the following analysis, one can see that equation (2) is inadequate for a complete description of that form which the human operator forces his open loop "descriptive function" to assume. Unknowns, such as P, N, and $\underline{J}$, will have to be algebraically eliminated in order to derive an expression for $\underline{H}$. Consider the following relations that follow from Figure 5.

$$E = F - \underline{J}\,C - P \tag{3}$$

$$C = \underline{H}\,E + N \tag{4}$$

The noises F, N, and P are linearly uncorrelated, but F, E, and C are dependent.

As an aside it might be mentioned that the above use of Fourier transforms is not rigorous, since the Fourier transform does not converge for a stationary time series. One can circumvent this problem by taking the transform of a function which is equal to the noise being studied in the interval $-T < t < T$, and which is zero elsewhere. The interval 2T covers a suitably long duration of time. In this fashion rigor may be approached and the results will be independent of the time interval for large enough T.

Starting with equations (3) and (4), an expression for $\underline{H}$ will now be derived,

$$E = F - \underline{J}\,\underline{H}\,E - \underline{J}\,N - P, \tag{5}$$

$$E = \frac{F - \underline{J}\,N - P}{1 + \underline{H}\,\underline{J}} \qquad (6)$$

and similarly by substitution and transposition

$$C = \frac{N + \underline{H}\,F - \underline{H}\,P}{1 + \underline{H}\,\underline{J}} \qquad (7)$$

The cross spectrum of two signals, X(t) and Y(t), can be defined as the expected value of the product of the Fourier transform of one function and the Fourier transform conjugate of the other function, or $\overline{X(\omega)Y^*(\omega)}$. This definition parallels the common definition of the power spectrum of X(t) as the expected value of $X(\omega)^2 = \overline{X(\omega)X^*(\omega)}$; the average being taken over an ensemble of noises X(t) (Ref. 15). In the particular computations described in this report the ergodic property of the assumed stationary time series was used so that the average was made over time, rather than over an ensemble of noises. Thus, since spikes in the frequency domain transform into long flat box-car-like functions in the time domain, time averaging of several successive sections of the time function is equivalent to averaging the corresponding Fourier transforms over a narrow band of frequencies. It can be seen, therefore, that

$$\underline{\bar{\Phi}}_{CF}(\omega) = \overline{CF^*} \qquad (8)$$

where the averaging is carried out over a narrow frequency band. Henceforth the notation $\underline{\bar{\Phi}}_{xy}$ will replace $\underline{\bar{\Phi}}_{xy}(\omega)$.

One can expand Equation (8) so that

$$\underline{\bar{\Phi}}_{CF} = \overline{CF^*} = \overline{\left(\frac{N + \underline{H}F - \underline{H}P}{1 + \underline{H}\underline{J}}\right) F^*} \qquad (9)$$

$$\underline{\bar{\Phi}}_{CF} = \frac{\overline{NF^*} + \underline{H}\overline{FF^*} - \underline{H}\overline{PF^*}}{1 + \underline{H}\underline{J}}$$

Because of the assumption of no correlation between the noises F, N, and P,

$$\overline{NF^*} = \overline{PF^*} = 0 \quad \therefore \quad \underline{\bar{\Phi}}_{CF} = \frac{\underline{H}\,\underline{\bar{\Phi}}_{FF}}{1 + \underline{H}\underline{J}} \qquad (10)$$

Similar reasoning demonstrates that

$$\underline{\bar{\Phi}}_{EF} = \frac{1}{1 + \underline{H}\underline{J}}\,\underline{\bar{\Phi}}_{FF} \qquad (11)$$

Consequently

$$\underline{H} = \frac{\underline{\bar{\Phi}}_{CF}}{\underline{\bar{\Phi}}_{EF}} \qquad (12)$$

Equation (12) defines the measurements which will have to be made to determine $\underline{H}$.

A note is in order with regard to azimuth error and azimuth control of the airplane. Both the aileron and rudder control the airplane in azimuth, so that there are really two control responses for this error signal component. The rudder control response, however, has been ignored in order to eliminate treating two sets of control responses. This seems reasonable: first, because aileron and rudder action should be well correlated; and second, because of the pilots' own testimony to the effect that they use practically no rudder to effect control of a fast jet such as the F-80 (Ref. 11).

Clearly, three signal channels, c(t), f(t), and e(t) are required to measure $\underline{H}$, the open loop "descriptive function", in each dimension. The two dimensional problem which was treated would thus require six recorder channels for the simultaneous measurement of $\underline{H}$ in each of two dimensions. The four channel recorder was decided upon when project thinking was centered on equation (2) as the defining relationship. The fact that the data handling is limited to four recording channels imposes cumbersome experimental restrictions which require separate measurements of elevator and aileron responses. It is well to point out that $\underline{H}'$, defined in equation (2), is the closed loop system pseudo "transfer function" for this particular problem in which N and P are not considered, and where $\underline{J} = 1$, rather than the open loop pseudo "transfer function" for the man. $\underline{H}'$, for the tracker, is related to $\underline{H}$ as follows:

$$\underline{H}' = \frac{\bar{\Phi}_{CF}}{\bar{\Phi}_{FF}} = \frac{\underline{H}}{1 + \underline{H}} \tag{13}$$

If we are interested in the open loop gain, G of the whole system, we must first obtain an expression for $\underline{J}$. Following algebraic manipulations much like those in equations (9-12). We find that

$$\underline{J} = \frac{\bar{\Phi}_{FF} - \bar{\Phi}_{EF}}{\bar{\Phi}_{CF}} \tag{14}$$

Equation (14) is an interesting result in itself since it represents the only way in which the transfer function of the simulator can be measured. This is because the simulator has to be measured when the loop is closed.

To get the open loop gain of the system, $\underline{G}$, we multiply $\underline{J}$ and $\underline{H}$.

$$\underline{G} = \underline{HJ} = \frac{\bar{\Phi}_{CF}}{\bar{\Phi}_{EF}} \cdot \frac{\bar{\Phi}_{FF} - \bar{\Phi}_{EF}}{\bar{\Phi}_{CF}} \tag{15}$$

$$\underline{G} = \frac{\bar{\Phi}_{FF}}{\bar{\Phi}_{EF}} - 1$$

Equations (13) and (15) are useful if we want to plot Nyquist diagrams to study system stability.

Since both $\underline{H}$ and $\underline{H}'$ represent that part of the performance that may be extracted by a linear correlation it is of interest to compute the magnitude of this correlation. Disregarding finesse, one finds that the equivalent linear correlation coefficient for a system operating as a closed loop is:

$$\rho_{CF} = \frac{|\bar{\Phi}_{CF}|}{\sqrt{\bar{\Phi}_{CC}\,\bar{\Phi}_{FF}}} \qquad (16)$$

If one prefers to think in terms of a signal to noise ratio, the following must be considered.

The noise at the output of the system is not $\bar{\Phi}_{NN}$ but rather $\bar{\Phi}_{NN}$ reduced by a factor analogous to the $(1-\mu\beta)^2$ term in feedback amplifiers. On the intuitive level, this means that the pilot responds to and corrects his own noise output when it is displayed before him on the scope. One would expect at least part of $\bar{\Phi}_{NN}$ to act like a muscle tremor; i.e., to be independent of input amplitude.

Defining output noise as $\bar{\Phi}'_{NN}$

then

$$\bar{\Phi}'_{NN} = \frac{\bar{\Phi}_{NN}}{|1 + \underline{HJ}|^2} \qquad (17)$$

Removing the linearly correlated part of $\bar{\Phi}_{CF}$, which is $|\bar{\Phi}_{CF}|^2/\bar{\Phi}_{FF}$ and bunching the uncorrelated part of the response which is due to nonlinearities in with the noise, one obtains

$$\bar{\Phi}'_{NN} = \bar{\Phi}_{CC} - \frac{|\bar{\Phi}_{CF}|^2}{\bar{\Phi}_{FF}} \qquad (18)$$

From the foregoing and equation (16) the signal to noise power ratio is, signal/output noise $= \rho^2_{CF}/1 - \rho^2_{CF}$

C. SIMPLE MATHEMATICAL MODEL FOR HUMAN OPERATORS

The foregoing section has derived the functional relations of interest in measuring "descriptive functions" as well as demonstrated the measurements which are needed. In this section we will make some guesses about what $\underline{H}$ might be expected to be for a simple case. These guesses will be made so that a simple mathematical model will be available for comparison with our data. The reader should always bear in mind that expressions for the operator's "descriptive function" are limited, in a

strict sense, to describing the measuring situation only--unless other empirical evidence extends their applicability. The major purpose of the experimentation described in this report is to determine the extent to which experimentally determined pseudo transfer functions can be made to describe different experimental conditions.

The following block diagram describes the simple tracking problem which this section will discuss.

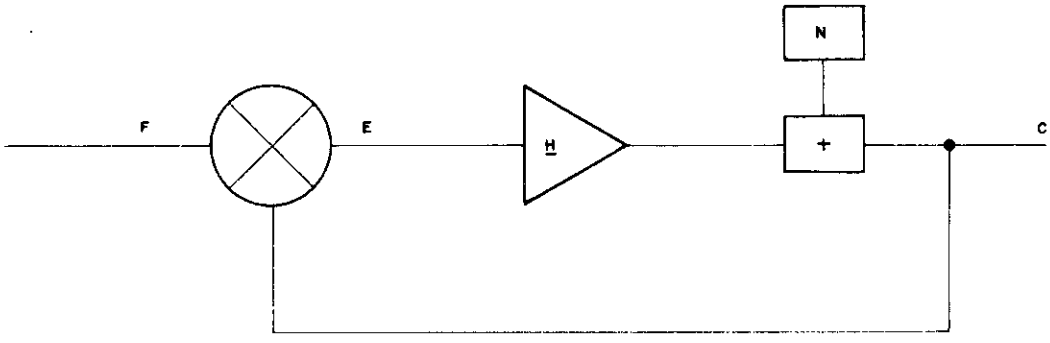

FIG. 5 — BLOCK DIAGRAM OF A SIMPLE TRACKING DEVICE

The conditions depicted in Figure 5 were obtained by degrading the aircraft simulator so that it acted like a simple two dimensional position tracking device.

It will be assumed that the human operator is primarily conscious of the final output and its relation to the input. The stimulus cues that are followed, or the amount of noise the human generates, is by-passed in the argument to be developed. In Figure 5 we have

$$E = F - C, \tag{19}$$

and

$$C = \underline{H}E . \tag{20}$$

The foregoing assumption states that the man is conscious only of the input, F, that produces an output, C, which follows E as closely as possible. From what we know of human tracking behavior the man will exhibit a reaction time lag, L, and he will be unable to hold the system gain, G, at unity. The system gain is G, where G is somewhat less than one. The foregoing then results in

$$C = G\, e^{-jL\omega} F, \tag{21}$$

from which we can see that the man must force his pseudo transfer function to be

$$\underline{H} = \frac{G\, e^{-jL\omega}}{1 - G\, e^{-jL\omega}} \qquad (22)$$

Experimental evidence (Ref. 15, 16) shows that G is a fairly flat function of frequency up to 2 or 3 times the input bandwidth after which G drops rapidly. In addition, G, which is always less than unity is a decreasing function of increasing input bandwidth. With these facts in mind we will hypothesize a G, which the operator might impose on himself (Fig. 6).

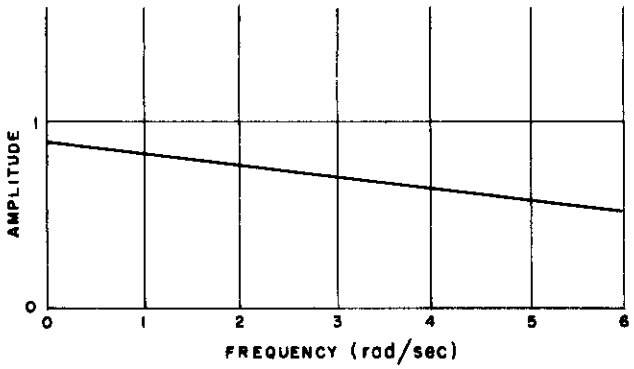

FIG. 6 — A HYPOTHESIZED GAIN FUNCTION

In Figure 6, G = 0.9 at 0 cps, dropping linearly to G = 0.5 at 1 cps. It turns out that $\underline{H}$ is not extremely sensitive to the shape of the curve in Figure 6. Furthermore, we assume a lag, L, of 0.3 seconds.

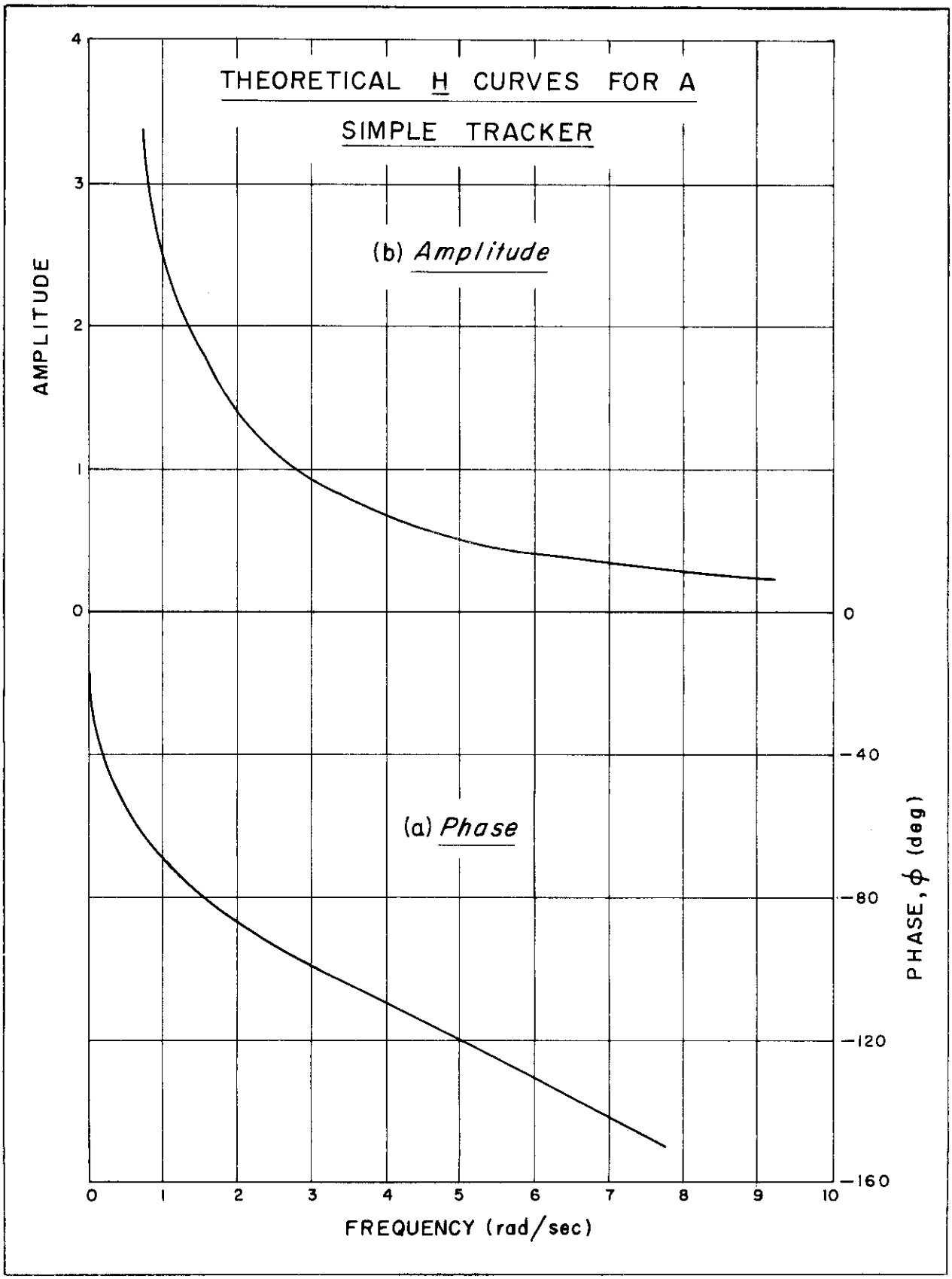

REPORT WADC TR 54-370 FIGURE 7

Figures 7a and 7b follow from equation (20) and illustrate the form which H would be forced to take were the human operator behaving according to the foregoing assumptions. Of course, since this report describes an experimental attempt to study H, the foregoing theorizing is, in a sense, out of place. Experimental data are easier to handle when their conformity or disagreement with expected results is possible. This is especially important when the data reduction procedure is, on occasion, in error. It is for these reasons that theoretical schemes were essayed.

D. CHECKING THE SIMPLE MODEL

Prior to conducting experiments with jet pilot subjects, a series of minor studies were conducted using Franklin Institute personnel as the subjects. These experiments were made for the purpose of checking procedures as well as insuring that it was meaningful to manipulate the experimental variables suggested for the experiments with pilots as subjects. Since the subjects for these preliminary experiments were non-pilots and also since it was convenient in reducing the data, the simulator was instrumented as a simple position tracking device (Fig. 5). An incidental use of the data will be an attempt to check the theoretical results that are predicted in Figures 7a and b.

Two subjects, Gl and Kr, who were experienced in operating the simulator when instrumented as a stick controlled tracking device, tracked three different two dimensional displays. Only aileron control, i.e., the horizontal dimension, was analyzed. The three displays had the same amplitude on the CRO, 0.6 inches rms, but they differed in that the forcing function bandwidths were variously 1, 2, and 4 rad/sec. The forcing functions in azimuth and in elevation had the same statistics; computations were carried out for the azimuth inputs and the aileron outputs only. The control parameters were 1.2 inches CRO deflection in azimuth for a stick movement in aileron of one inch, and 3.2 inches CRO deflection in elevation for an elevator movement of one inch. (Since the hand grip on the stick was about 28 inches long and the scope face was about 28 inches from the subject, the foregoing control ratios are numerically equal for degrees or inches.) The forces on the stick were the same as for the case where an aircraft was simulated, with 1.25 pounds per degree for aileron control and 21 pounds per degree for elevation control. The stick was the only means the subject had of controlling the pip. Although both subjects were experienced operators, i.e., about half an hour of simulator time with all three bandwidths, previous to this experiment, we allowed a one minute warm up period with the 2 rad/sec input signal after which the recorded runs were begun. The presentation order was 1, 4, and 2 rad/sec bandwidths. There was a three minute pause between runs and each run lasted two minutes (Fig. 8). Due to data reduction difficulties one run had to be discarded.

A FAMILY OF H CURVES FOR THE SIMPLE TRACKER

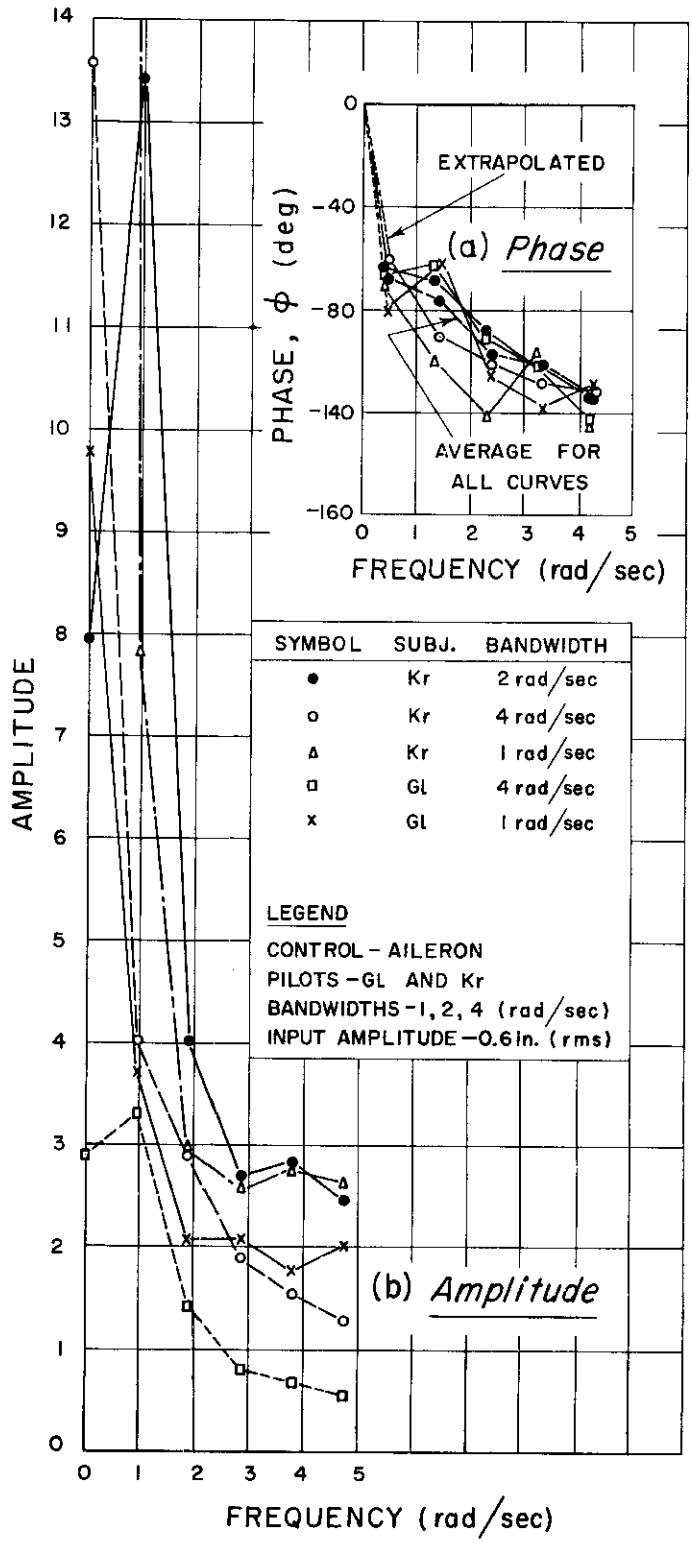

REPORT WADC TR 54-370

FIGURE 8

The apparent lag in Figure 8a is approximately 0.24. There is no point in belaboring the similarity of Figures 7 and 8 since the curves make it clear that the method used gives results which are reasonable when compared with the highly simplified model. As measured from $\bar{\Phi}_{CF}$ slopes (Figs. 37 and 38 in Appendix II), the following reaction time averages over frequency were noted.

Subject	Bandwidth rad/sec	Reaction time seconds
Kr	1	0.34
Kr	2	0.22
Kr	4	0.28
Gl	1	0.35
Gl	4	0.42

E. ATTEMPTS AT GETTING A MATHEMATICAL MODEL FOR JET PILOTS

Attempts to obtain simple models which describe the form which the human operator forces his pseudo transfer function to assume when he is flying the simulator have not been uniformly successful. A few of the attempts that were made are sketched below.

Assume that $\underline{J}$ in Figure 5 is replaced by $\frac{1}{j\omega}$. In other words assume that the airplane may be treated as a simple integrator. Again, by bypassing the operator on the simulator generated noises, one may write from Figure 5,

$$E = F - \frac{C}{j\omega}, \tag{23}$$

and by assumption

$$\frac{C}{j\omega} = G\, e^{-jL\omega} F, \tag{24}$$

therefore

$$\underline{H} \equiv \frac{C}{E} = \frac{j\omega G\, e^{-jL\omega} F}{F - \frac{Ge^{-jL\omega}}{j\omega} F} = \frac{j\omega G\, e^{-jL\omega}}{1 - Ge^{-jL\omega}} \tag{25}$$

Assuming that the human operator tracks with the same proficiency with the aircraft simulator as with the device in Figure 5, and assuming that G has the same form as in Figure 6, then Figures 9a and b show the phase and amplitude characteristics $\underline{H}$ must assume.

THEORETICAL H CURVES FOR THE AIRPLANE SIMULATOR

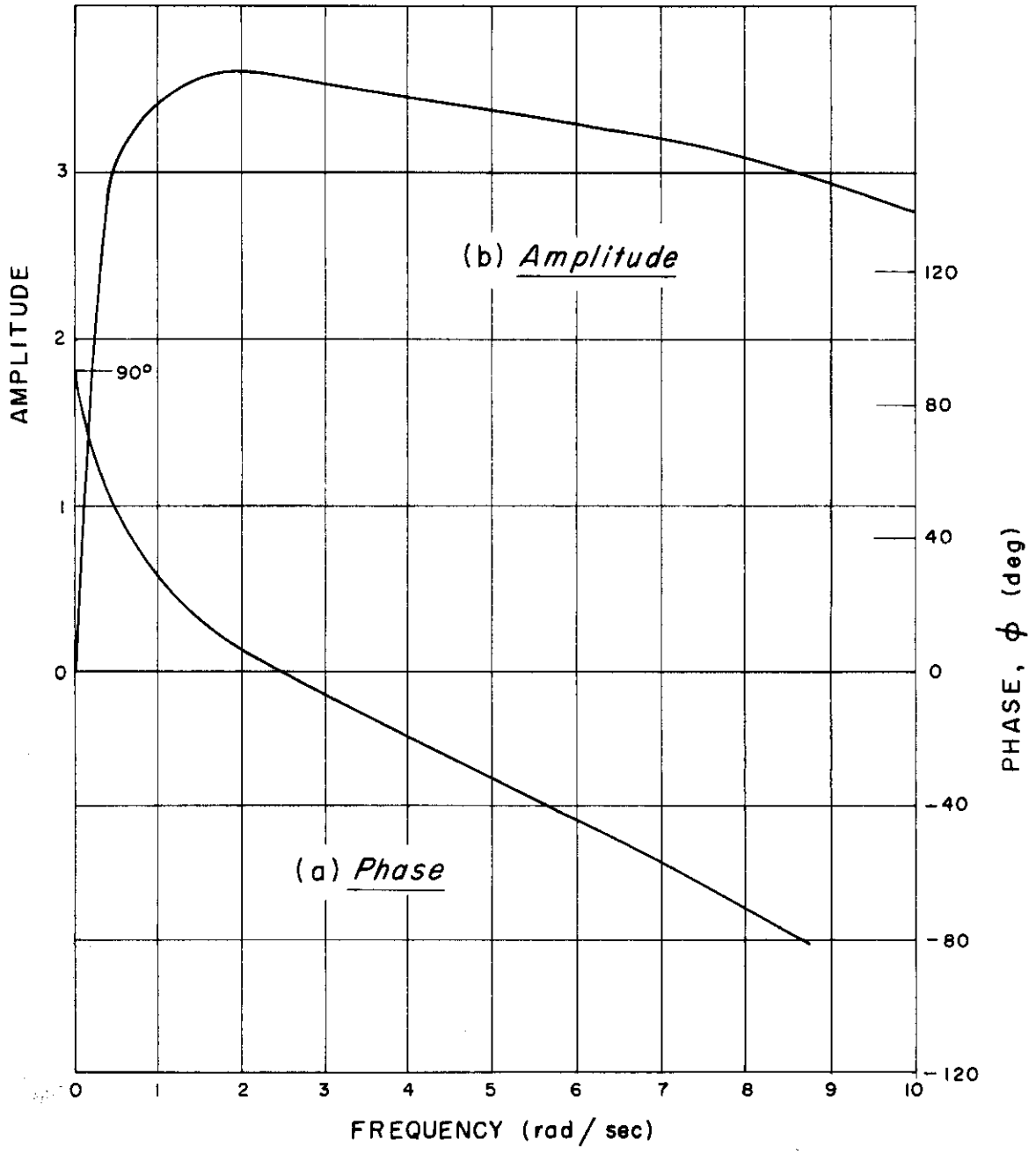

REPORT WADC TR 54-370 FIGURE 9

In a similar development one could change the assumptions so that G = 0.8 at 0 cps, dropping to zero at 1 cps, and further assume a reaction time delay of 0.667 seconds. The higher reaction time can be rationalized by hypothesizing an intervening mental process between stimulus and response in flying an airplane.

Figures 10a and 10b show the phase and amplitude curves for H, which follow from the foregoing assumptions.

Many other assumptions were made, none of which fared well when confronted with the data.

ALTERNATE H CURVES FOR THE AIRPLANE SIMULATOR

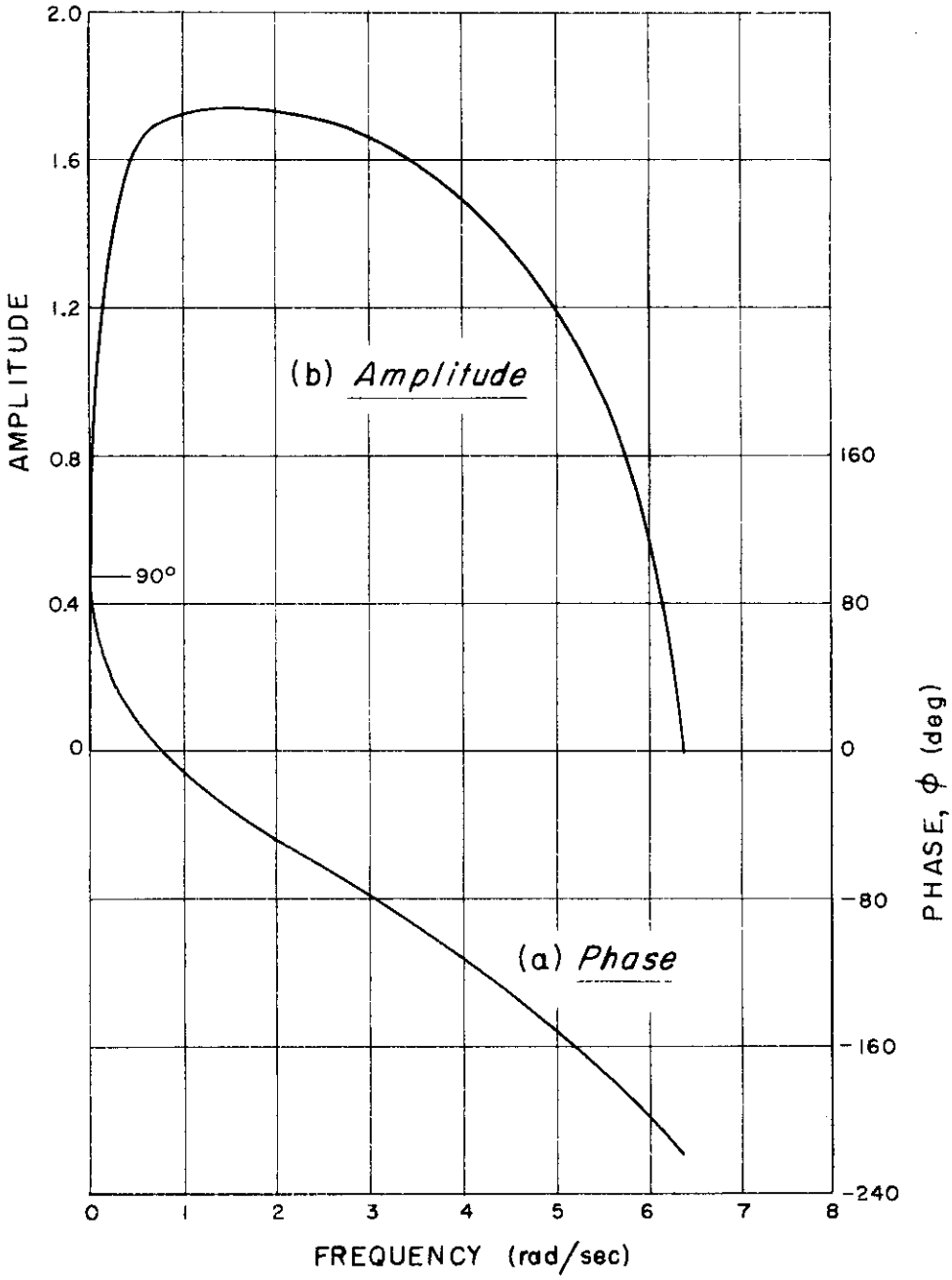

REPORT WADC TR 54-370

FIGURE 10

II. RESULTS

A. INTRODUCTION

The results which will be presented in this section consist of phase and amplitude characteristics for pilots flying an F-80A simulator. Four pilots were used as subjects. Each pilot was always presented a two dimensional random tracking problem which required that he exert both elevator and aileron control with his stick. In all cases the statistics for the random input in azimuth were the same as in elevation. Rudder control was not used.

A series of small balanced experiments was performed using the jet pilots as subjects; however, since the data reduction procedure was unreliable at times, many of these experiments were disrupted. Because of the lack of intact experiments designed to test hypotheses about pilot behavior, it became necessary to piece together data from various small experiments. Sufficient pieces of data were reshuffled so that experimental evidence could be presented. Because of the inordinate effort required, confidence limits have not been computed for the phase and amplitude plots. Rough estimates based on the arguments in Appendix III indicate that σ is about 15% of the dependent variable's value.

B. PRACTICE, PILOTS, AND INPUT AMPLITUDE COMPARISONS

The first experiment to be discussed was designed to determine the effects of distributed trial training with the simulator on the time stationarity of $\underline{H}$. Two pilots, Ap and Ha, were instructed to act as if the moving pip on the CRO were an enemy aircraft with which they were engaged in combat. The two pilots then spent a total of a half hour each on distributed trials of three to four minutes, during which they became familiar with the simulator. During this time each of the three bandwidths, 1, 2, and 4 rad/sec, were presented for durations of three to four minutes. The subject was equally trained in each bandwidth. The rms input amplitude on the CRO was 0.6 inches. This rms amplitude was the same for all bandwidths and was the same for azimuth and elevation.

Following the familiarization practice one pilot gratuitously commented on the four rad/sec program: "I'd never fire in air that gusty." The implication, verified by further informal questioning of both of the pilots, was that the 1 and 2 rad/sec bandwidths were reasonable approximations to gusty air actually encountered in firing runs.

The design of this and other experiments was complicated by the fact that the data reduction apparatus has a capacity of four signal channels; whereas three signal channels are required to characterize each dimension (Eq. 13). Consequently, phase and amplitude response curves can be computed for only one dimension of control (aileron or elevator) during each tracking trial. Accordingly, the following schedule was arranged for investigating time stationarity in the two control dimensions.

Forcing functions having two rads/sec bandwidth and an rms amplitude of 0.6 inches on the CRO were used in the trial runs. The statistics in azimuth and elevation were the same. The pilots were not told what was being recorded during any of the runs. The trials began with pilot Ap flying for two minutes while data were recorded which would enable the measurement of $\underline{H}$ for aileron responses to azimuth inputs. Following this trial, pilot Ha flew for two minutes while data were recorded for measuring $\underline{H}$ for elevator responses to elevation inputs. Pilot Ap then repeated his first run. The two pilots flew the simulator in this sequence until each man had made ten runs. Each pilot then made a second series of ten runs. This second series of ten runs differed from the first in that pilot Ap was recorded for elevator control responses and pilot Ha was recorded for aileron control responses.

The summary results from the foregoing trials are presented in Figures 11-14. Figures 29, 30, 32, and 33 in Appendix II illustrate the sort of data from which Figures 11-14 have been derived. Figures 32 and 33 in Appendix II illustrate the spread in the phase and amplitude characteristics. No significant differences were found between trials, hence the results are presented as averages in Figures 11-14.

Figures 11-14 are averages over trials and also averages for the reflected anti-symmetrical points (Fig. 29 and 30 in Appendix II). Since the data reduction apparatus did not consistently supply usable data, the number of individual trials averaged in Figures 11-14 was not always ten. While ten trials were averaged for Figure 11 and Figure 14, only six trials were averaged for Figures 12 and 8 in Figure 13.

The validity of Figures 11-14 is independent of their conformity with the mathematical models of the foregoing section. It is, however, of interest to note that Figures 11 and 12 agree roughly with Figure 10. The $\phi = 90°$, $\phi = 0$ points on Figures 11a and 12a are extrapolated. Measurements made beyond the input bandwidth of two radians are suspect since the linear correlations computed from equation (15) tend to be lower than .5 at these frequencies. The reader may be surprised at the apparent increase in gain exhibited by the pilots as frequency increases. This increase may be an artifact since equations (III.36) and (III.37) indicate a huge increase in confidence limits as $\bar{\Phi}_{FF} \to 0$ and $\bar{\Phi}_{NN}$ becomes large. In fact, as the frequency goes far enough beyond the upper limit of the input bandwidth, the linear model breaks down.

AVERAGED H CURVES, AILERON – PILOT Ap

LEGEND
CONTROL – AILERON
PILOT – Ap
BANDWIDTH – 2 (rad sec)
INPUT AMPLITUDE – 0.6 in (rms)

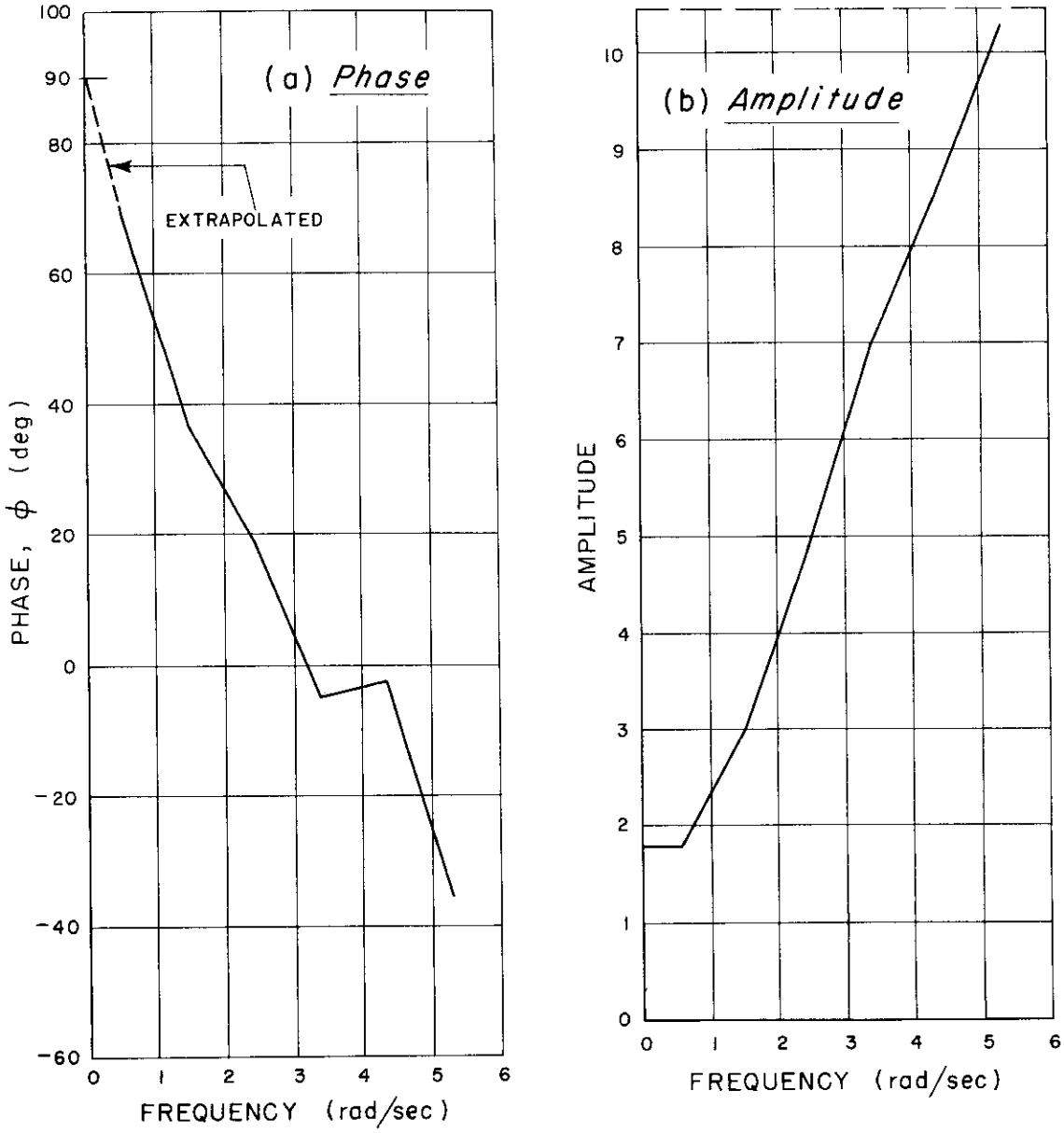

REPORT WADC TR 54-370

FIGURE 11

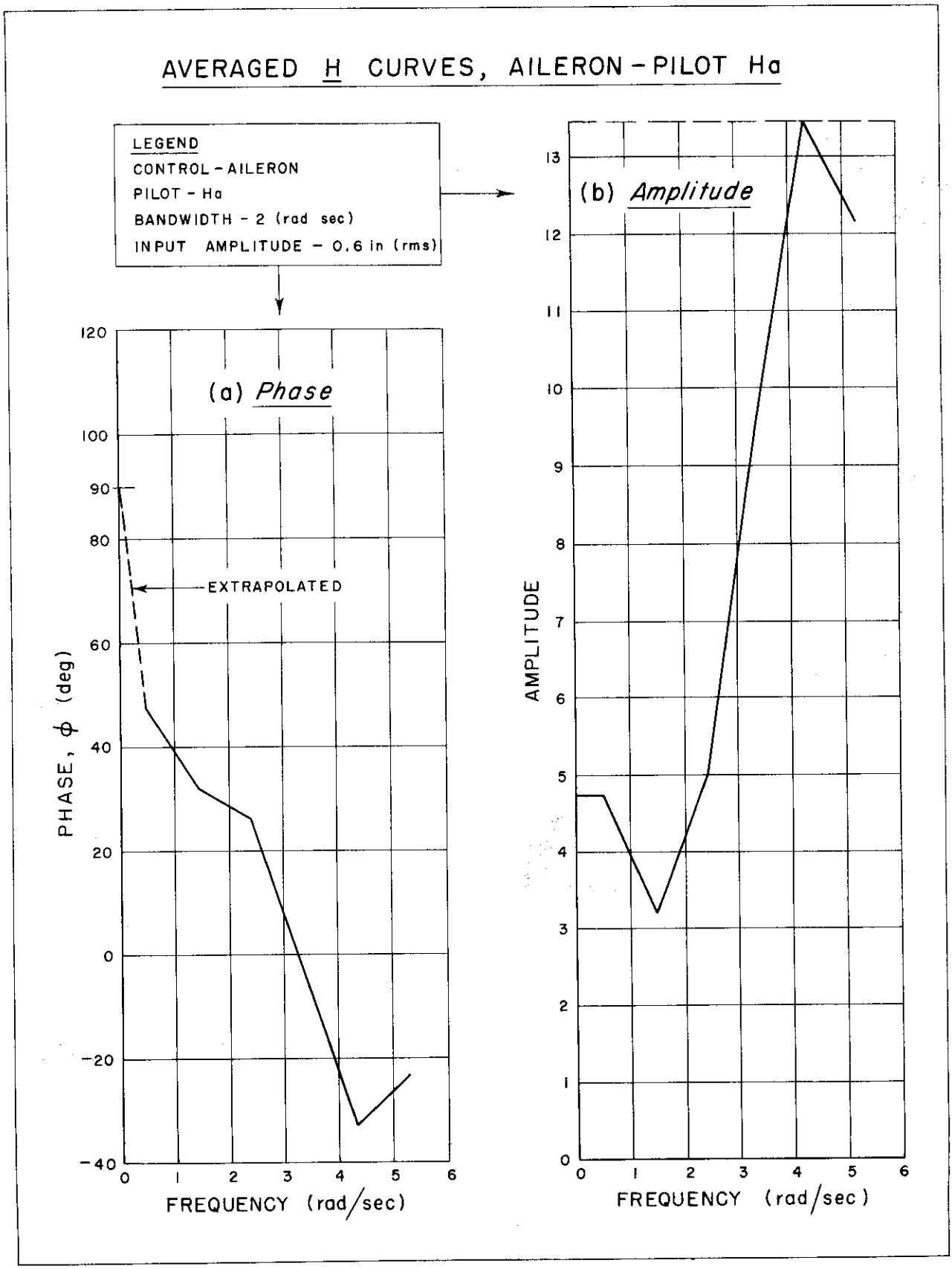

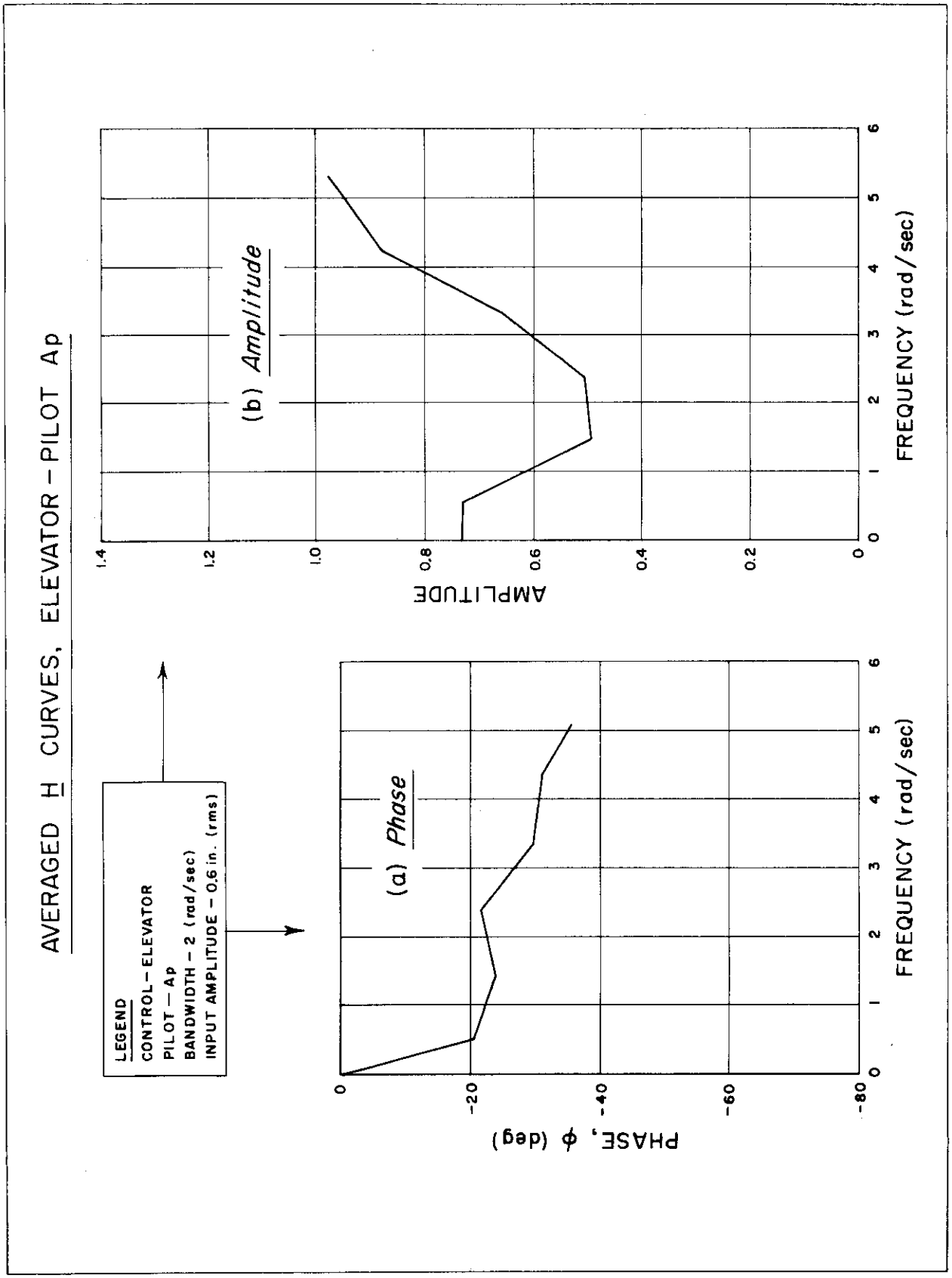

REPORT WADC TR 54-370

FIGURE 13

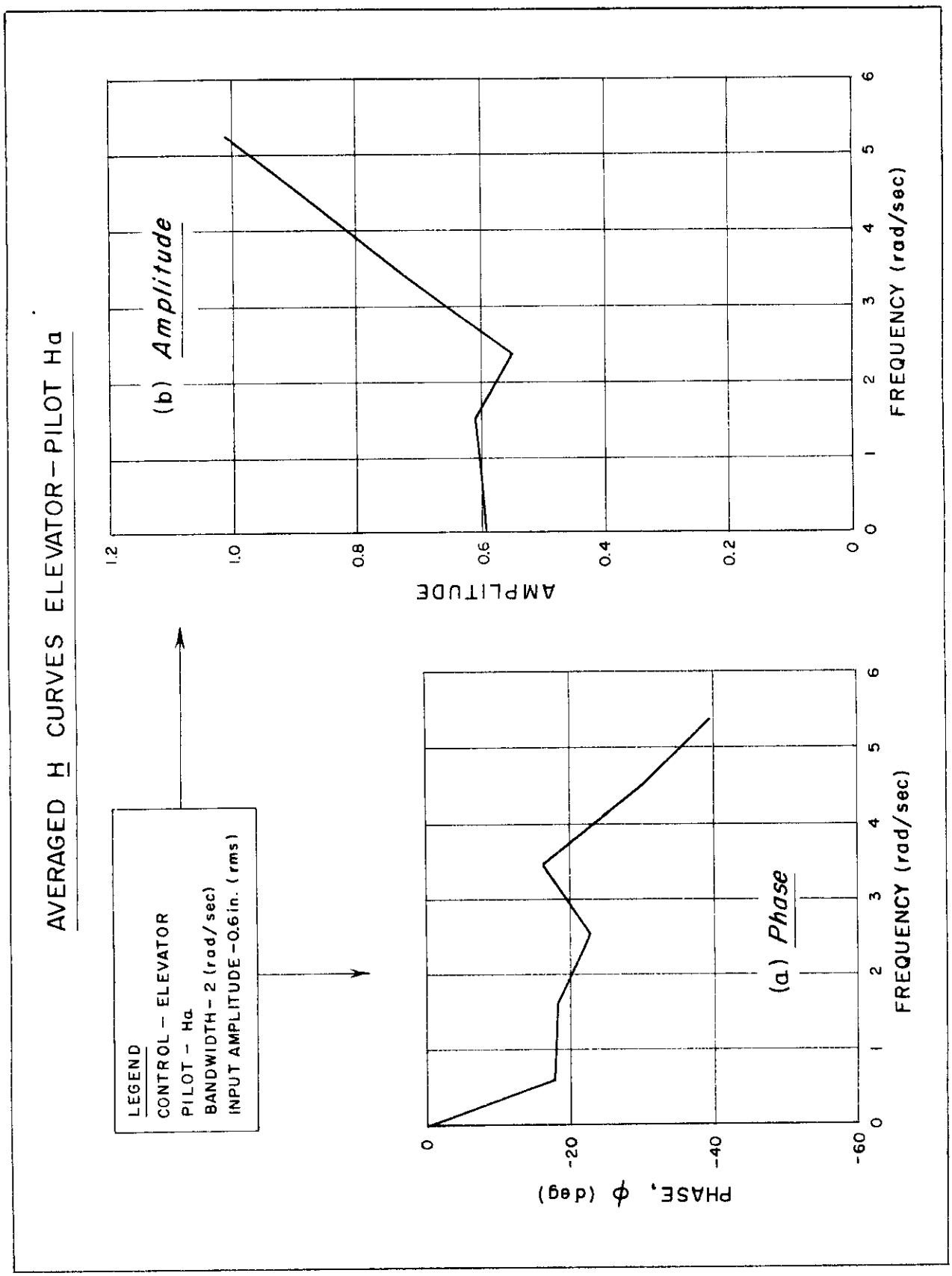

REPORT WADC TR 54-370

FIGURE 14

Two important results can be found in Figures 11-14, outside of the fact that this experiment indicated the pilot's behavior was time stationary under the measurement conditions. First, in comparing Figure 11 with 12 and Figure 13 with 14 we see a striking similarity between the pilots. Second, in the comparison of figures 11 and 12 with Figures 13 and 14 it clearly illustrates how $\underline{H}$, which the pilot imposes on himself when responding to an azimuth signal, differs from that $\underline{H}$ imposed when responding to an elevation signal. Of course, the shapes of the curves in Figures 11-14 are in themselves the main result.

As a matter of curiosity, one might compare the average reaction times for the two pilots Ap and Ha when responding with elevator and aileron control. These reaction times are obtained by averaging the slopes of the $\bar{\Phi}_{CF}$ plots. See Figures 29 and 30 in Appendix II. The average reaction times corresponding to Figures 11, 12, 13 and 14 are 0.62, 0.80, 0.27, and 0.29 second. Although reaction time differences between pilots are not statistically significant, differences between reaction times for aileron and elevator are highly significant. Phenomenally, elevator control has relatively little lag, whereas aileron control is sluggish. The pilot may use part of the greater reaction time in aileron to engage in short term prediction of the target position.

In the following paragraphs a series of experimental comparisons will be made between $\underline{h}$ values measured under differing conditions.

The first experiment described does not exhaust the manner in which time variations could influence $\underline{H}$. Figures 15 and 16 represent measurements made on $\underline{H}$ at the beginning and at the end of a continuous six minute session in the simulator. For both Figures 15 and 16 the pilot was Wa, who had about an hour's practice with the simulator prior to the taking of these measurements. The forcing function for Figures 15 and 16 was of 0.6 inches rms amplitude on the CRO, and of 2 rads/sec bandwidth. The statistics of the random input were the same in azimuth and in elevation. Figure 15 refers to elevator response characteristics. The number 1 denotes the curves for $\underline{H}$ measured over the first two minutes of the six minute run, and the number 2 denotes the curves for $\underline{H}$ measured over the last two minutes of the six minute run. Figure 16 refers to aileron response characteristics. The numbers 1 and 2 have the same meaning as in Figure 15. The number 3 denotes a curve obtained for the same pilot and the same input program one day later. The differences between the curves of Figure 15 and the differences between the curves of Figure 16 are not statistically significant.

Comparisons between performance on like tasks on successive days are found in Figures 17 and 18. In Figure 17 pilot Wa was the subject and in Figure 18 pilot Ra was the subject. For both pilots the input was a random noise source of 2 radian bandwidth and 0.6 inch rms amplitude. Both pilots tracked in two dimensions, but Figures 17 and 18 refer to the elevator responses. Records for the first and second day are denoted by the numbers 1 and 2. No statistical significance can be attached to these day-to-day variations. The high peak in the amplitude response, number 2 in Figure 18, is probably an artifact due to 120 cycle pick-up in the data reduction apparatus's modulator.

STATIONARITY COMPARISON, ELEVATOR

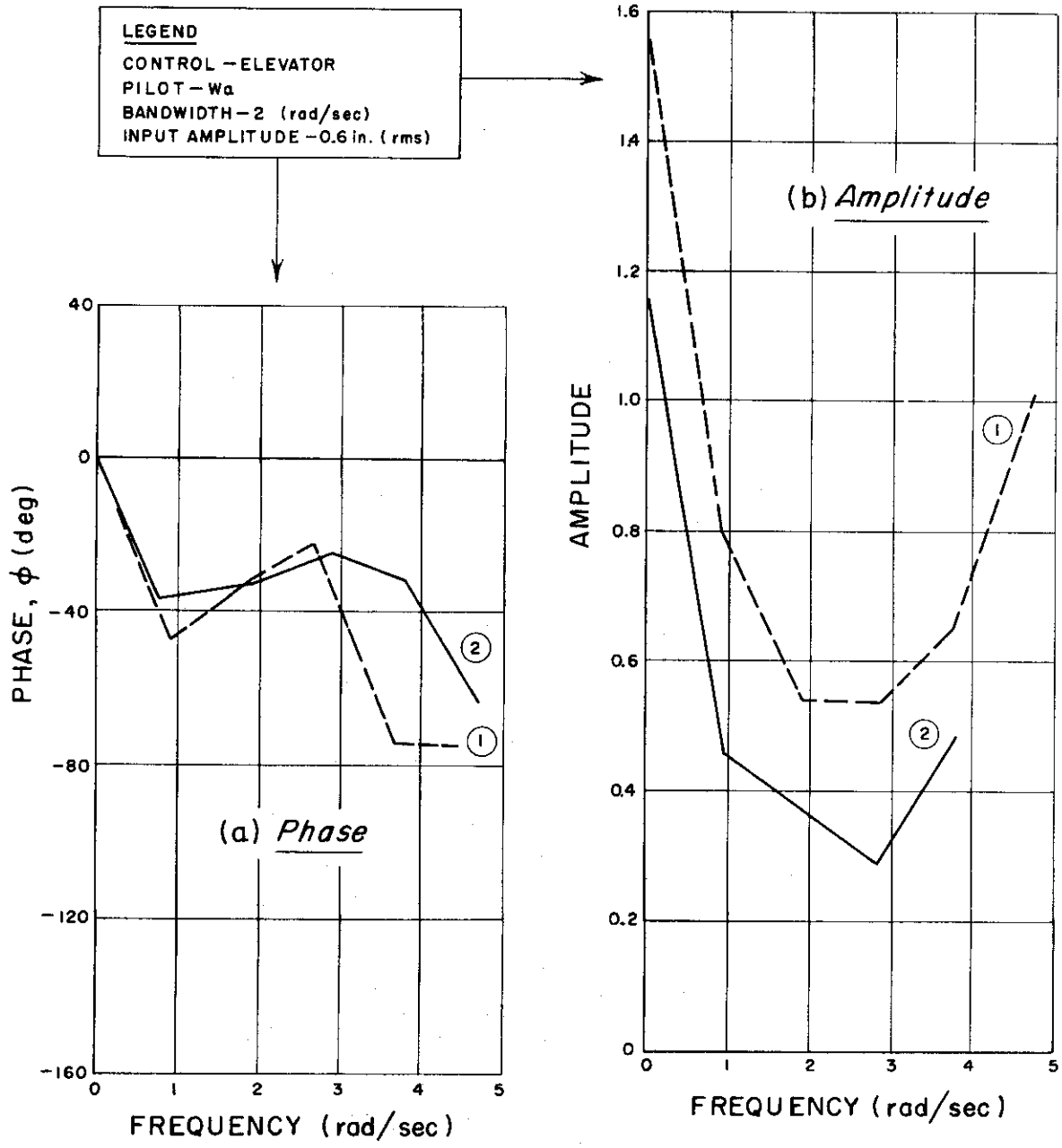

REPORT WADC TR 54-370

FIGURE 15

STATIONARITY COMPARISON, AILERON

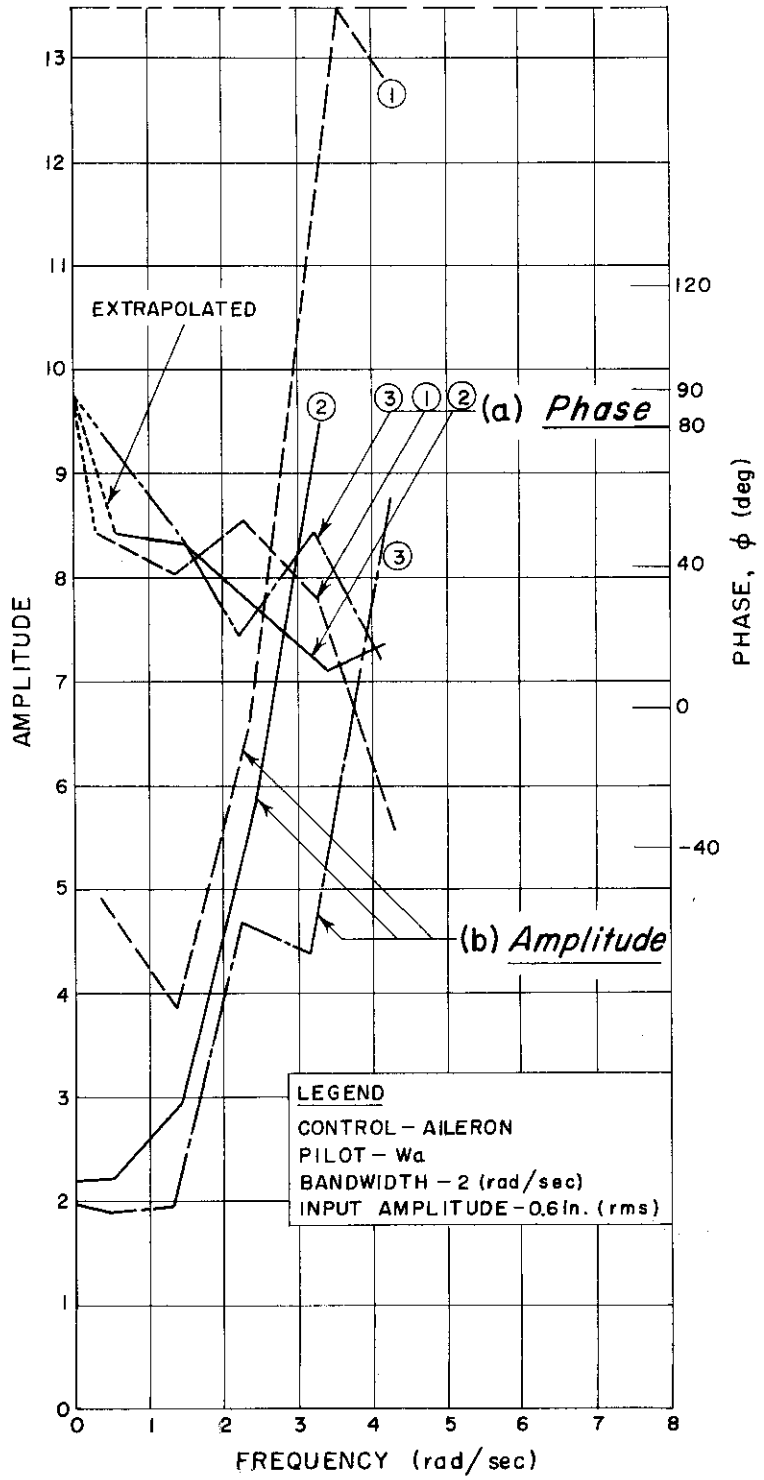

REPORT WADC TR 54-370

FIGURE 16

DAY-TO-DAY VARIATIONS, PILOT W_a

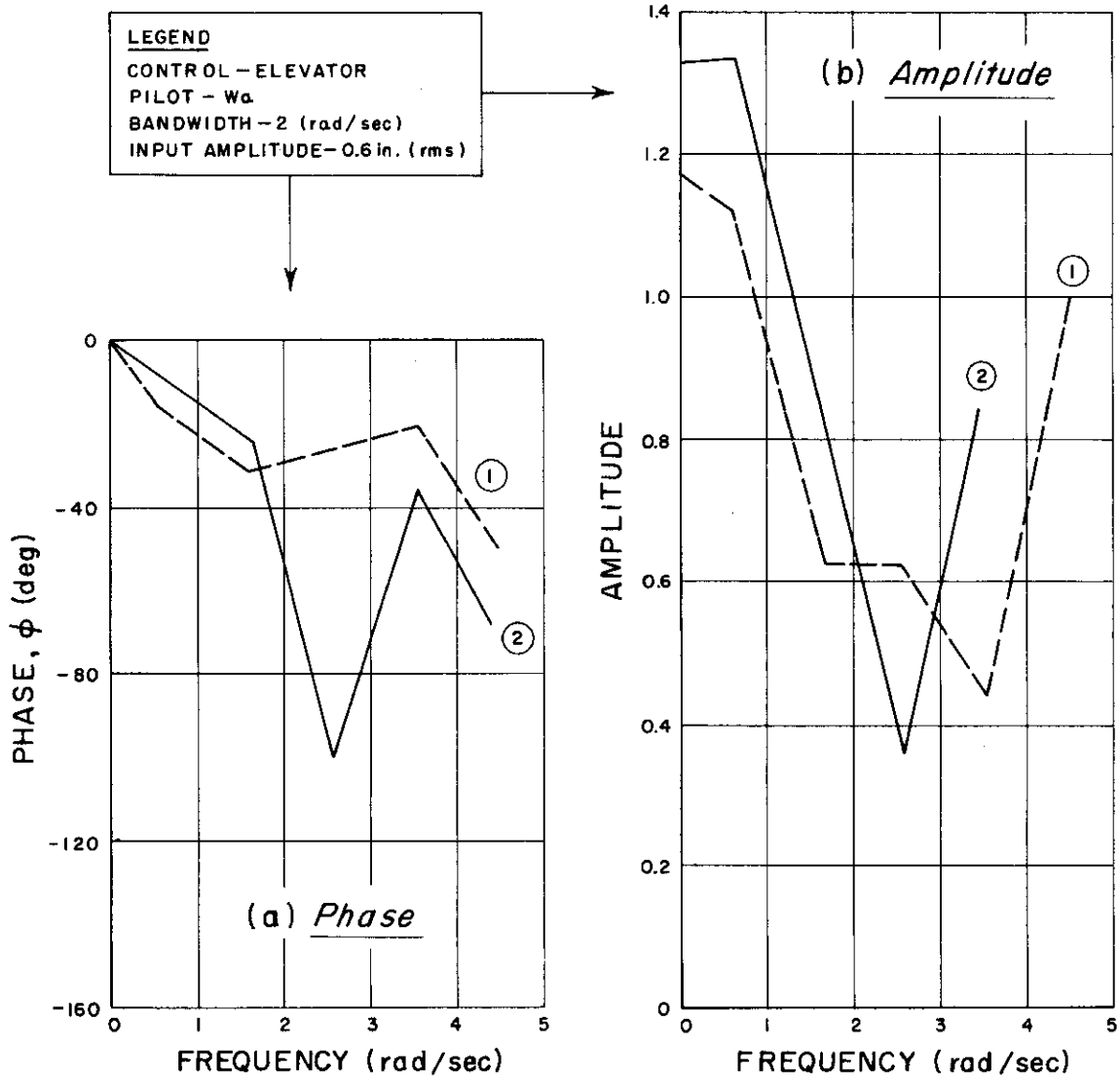

REPORT WADC TR 54-370 FIGURE 17

DAY-TO-DAY VARIATIONS, PILOT Ra

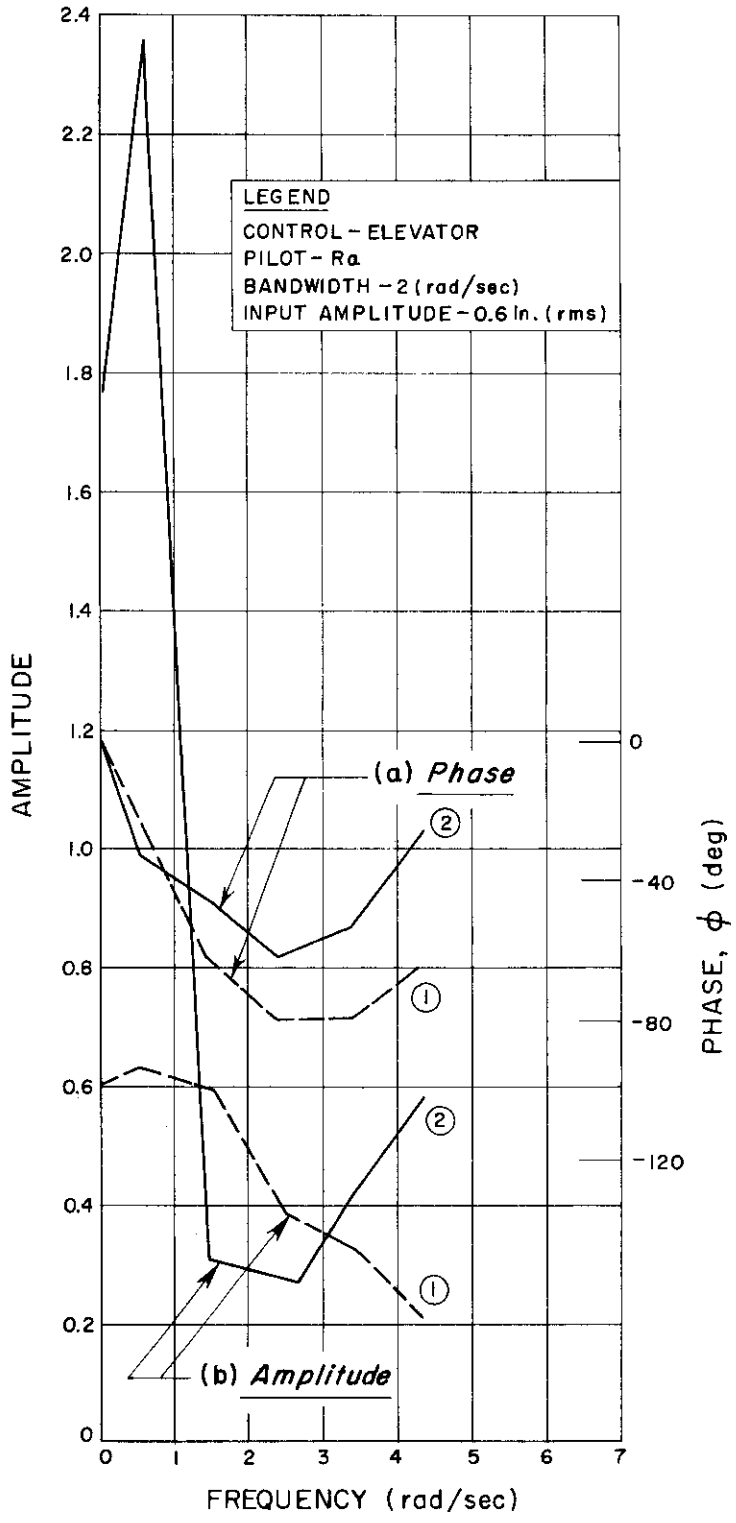

REPORT WADC TR 54-370

FIGURE 18

C. EFFECTS OF INPUT BANDWIDTH AND COMPARISONS OF SIMULATOR WITH SIMPLE TRACKER

In the following two comparisons input amplitude is an experimental parameter. Figure 19 shows three elevator response amplitudes and phase characteristics. Two pilots, Wa and Ra, served as subjects. Pilot Wa tracked a 2 rad/sec bandwidth, 0.3 inch rms amplitude forcing function. Pilot Ra tracked two successive forcing functions; both having a 2 rad/sec bandwidth. Pilot Ra's input 1 had an rms amplitude of 0.3 inches, and input 2 had an rms amplitude of 1.2 inches.

The comparison of runs 1 and 2 for Ra shows no significant difference in the phase response, although the amplitude plot has increased by approximately a factor of three. There is no statistically significant difference between the 0.3 inch rms flights for Ra and Wa.

Figure 20 shows aileron phase and amplitude plots for pilots Wa and Ra with a 2 rad/sec bandwidth and 1.2 inches rms amplitude forcing function. The differences in both phase and amplitude for pilots Wa and Ra are significant. It is of interest to note that individual differences crop up as we advance toward extreme conditions. A 1.2 inch rms amplitude consists of an unrealistically large series of excursions on the scope. It is of further interest to compare Figure 20 for pilot Wa with Figure 16 for pilot Wa flying a 2 rad/sec bandwidth forcing function of 0.6 inch rms amplitude. There is no significant difference between these curves.

In order to illustrate differences due to forcing function bandwidth changes, consider the following. It should be borne in mind that a four radian bandwidth input program is just marginally realistic and extremely difficult to fly. Figure 21 compares aileron control phase and amplitude responses, for pilot Ra, for forcing functions of bandwidth 1 rad/sec and an rms amplitude of 0.6 inches with responses to a forcing function of bandwidth 4 rads/sec and 0.6 inches rms amplitude. Note that we cannot be confident about any findings beyond about two radians bandwidth for the one radian input. Effectively we are limited to one significant point on that curve. Figure 22 shows aileron phase and amplitude responses for 4 rads/sec forcing function bandwidths and 0.6 inches rms amplitude. The data are due to pilots Ap and Ha. Compared with Figures 11 and 12, which are 2 radian bandwidth plots for the same pilots, the differences are at best marginally significant.

Figure 23 presents a comparison in the responses to the former 4 rads/sec 0.6 inch rms forcing function as encountered by Ap in the simulator and as encountered by Ap in the simple tracker. The comparison was prompted by the notion that perhaps Ap was responding in a more rigid and less adaptive fashion for the difficult and marginally realistic 4 radian input, making his responses somewhat similar for both tracker and airplane. Both the simulator and tracker curves in Figure 23 are representative of their populations, and the foregoing notion seems irrelevant. A more interesting comparison, presented for whatever it is worth, is shown in Figure 24. If the pilot holds the open loop gain of the feedback

INPUT AMPLITUDE COMPARISONS

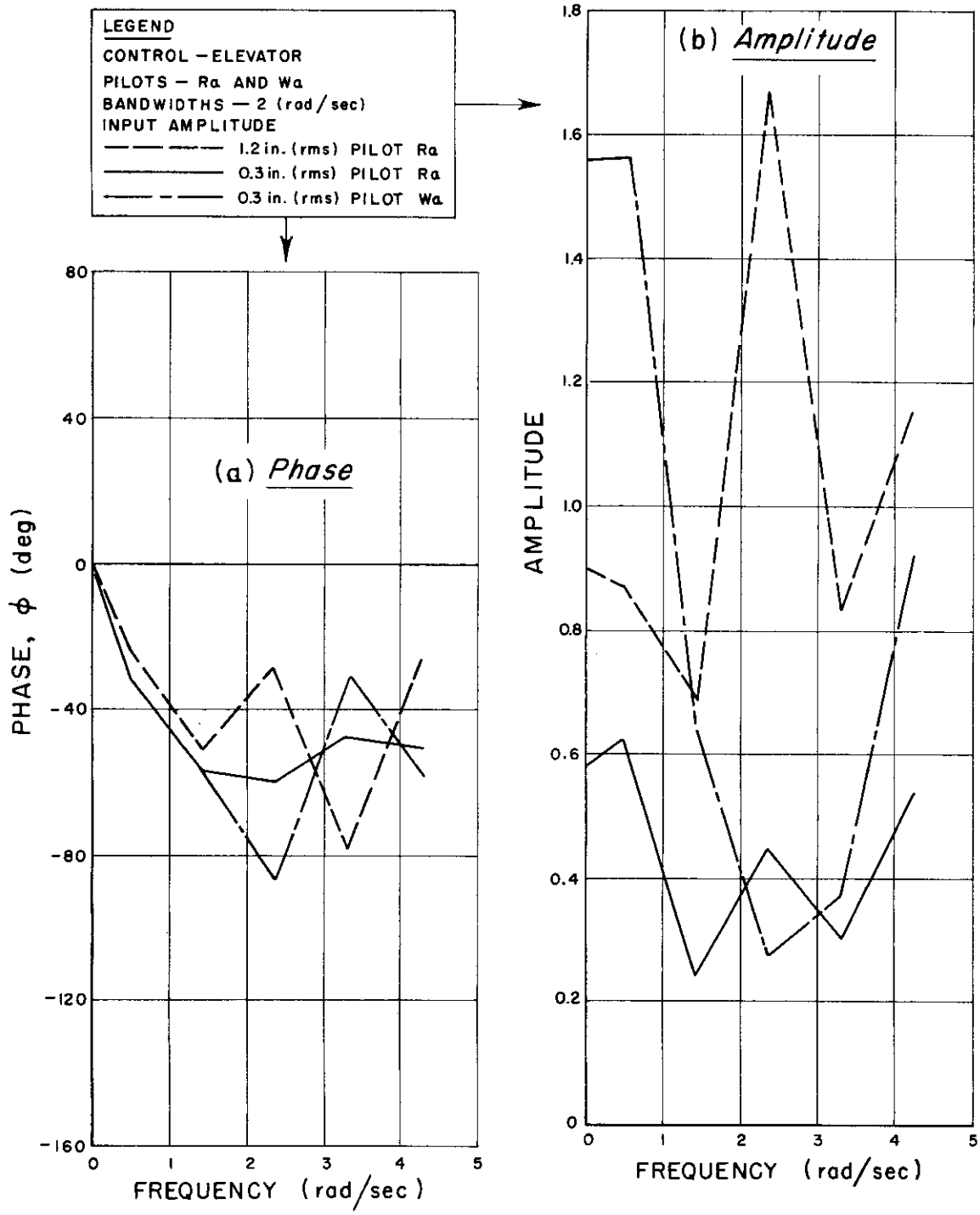

REPORT WADC TR 54-370 FIGURE 19

COMPARISON OF PILOTS Ra AND Wa

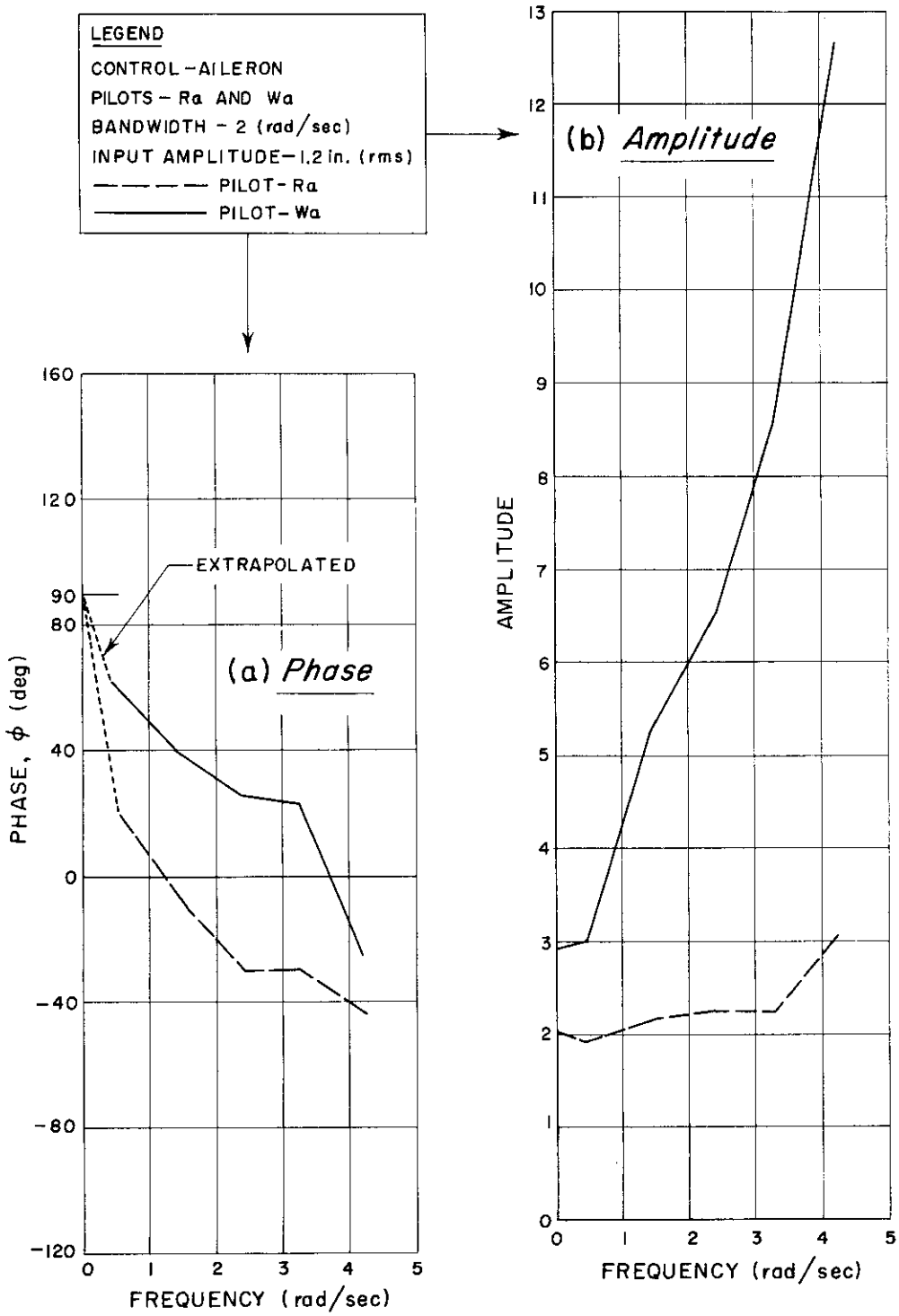

REPORT WADC TR 54-370

FIGURE 20

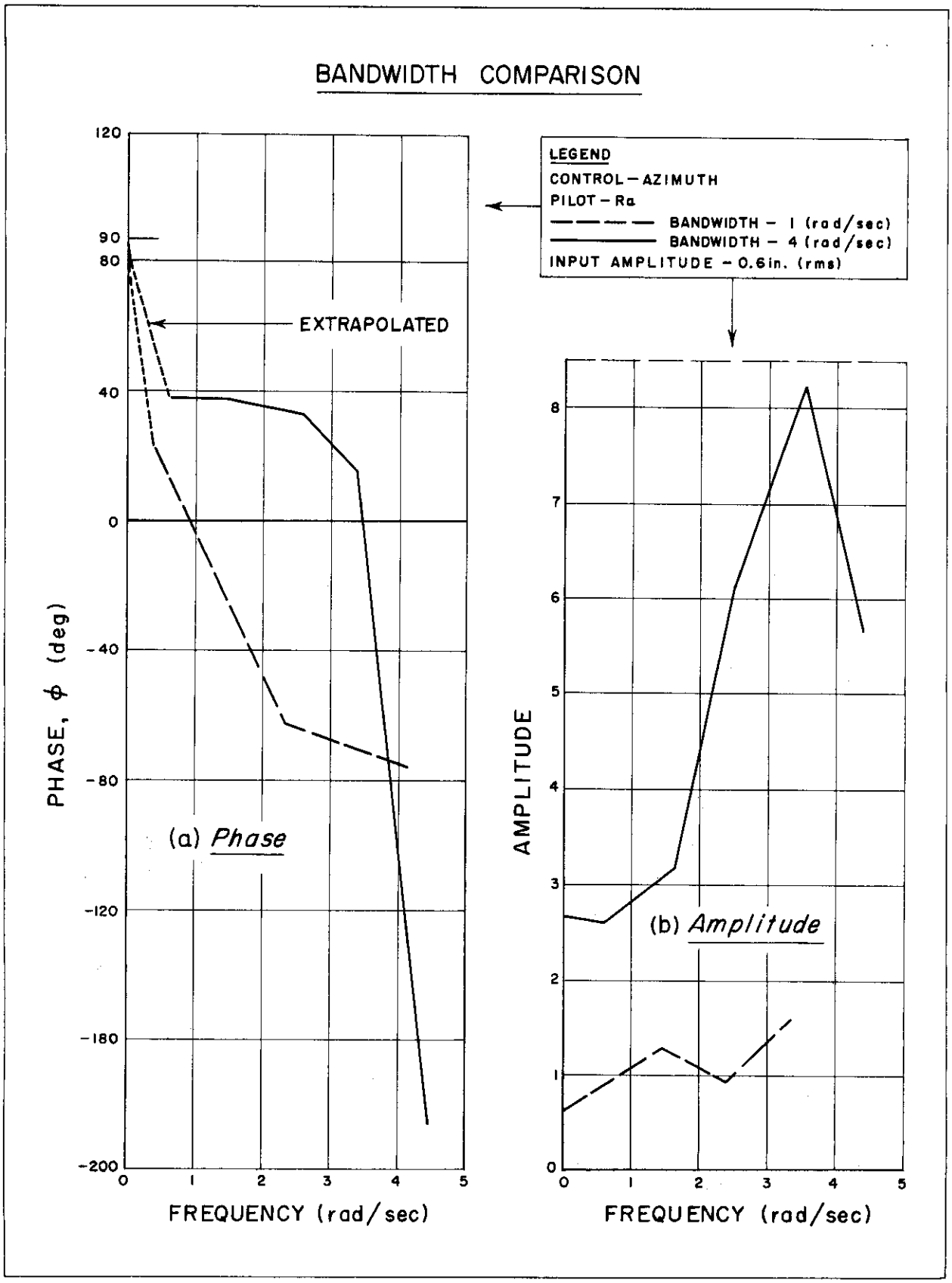

REPORT WADC TR 54-370 FIGURE 21

COMPARISON OF PILOTS Ap AND Ha

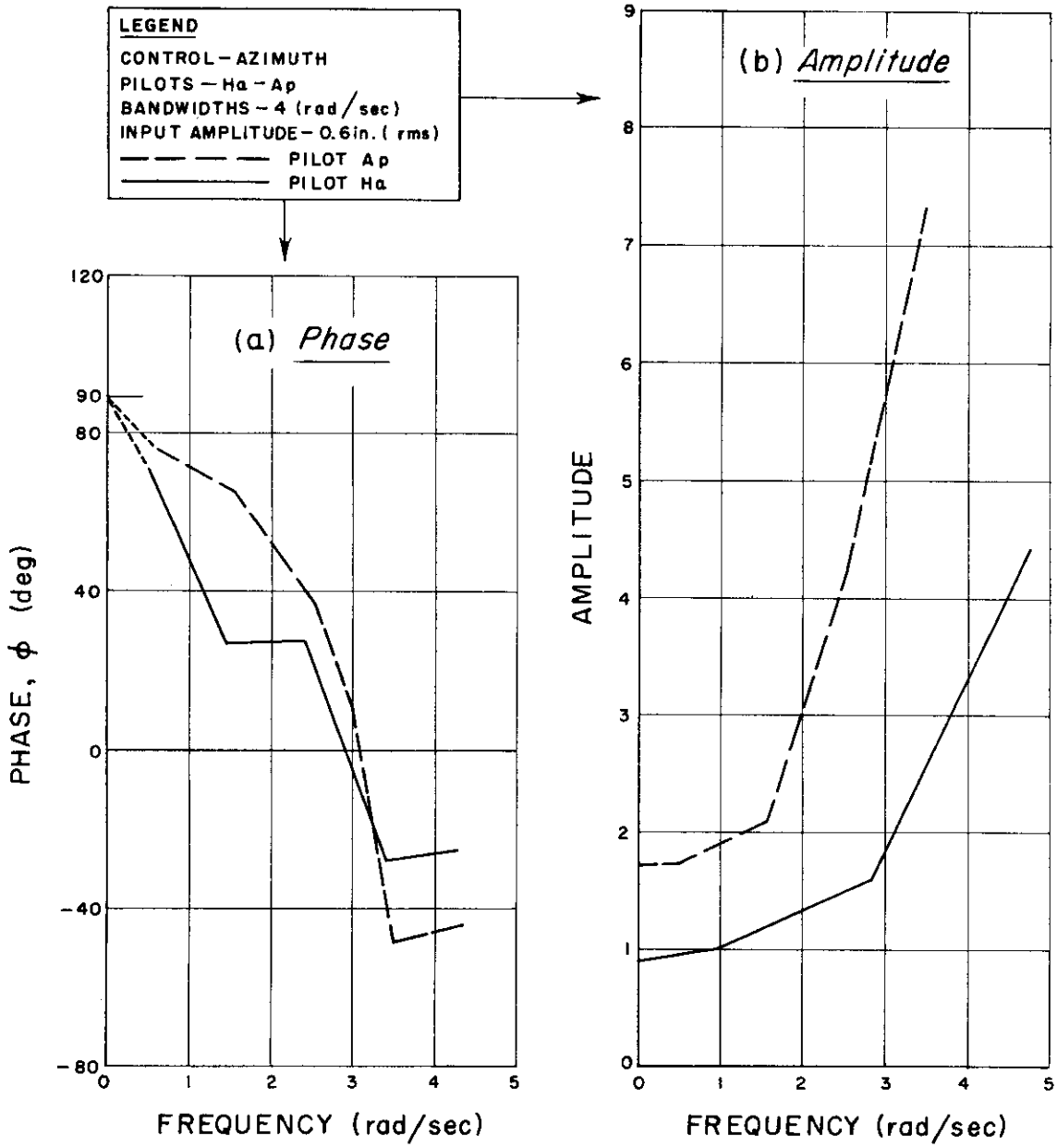

REPORT WADC TR 54-370 FIGURE 22

SIMULATOR AND TRACKER COMPARISON

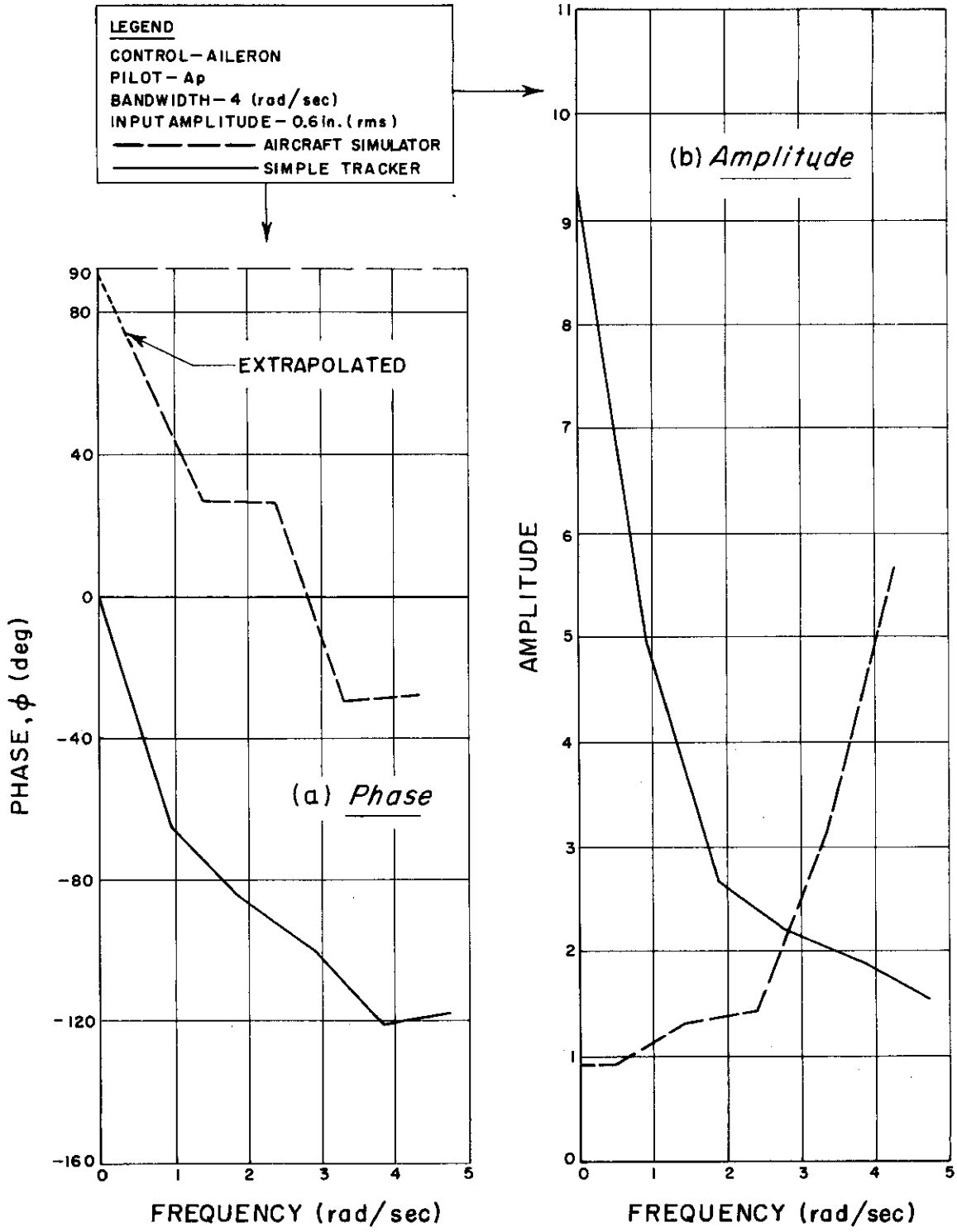

REPORT WADC TR 54-370

FIGURE 23

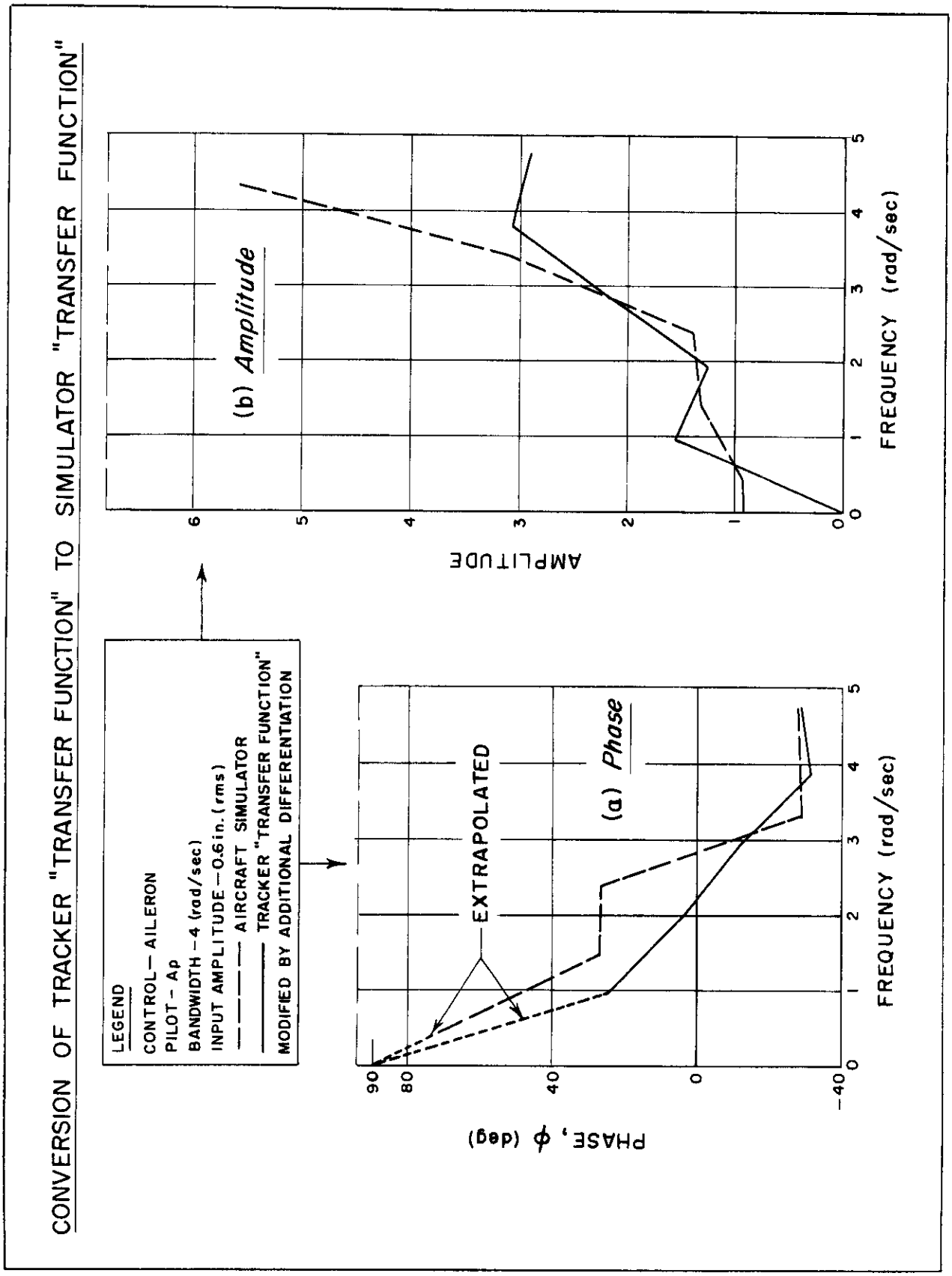

REPORT WADC TR 54-370

FIGURE 24

loop involved fairly constant, even though the feedback path is interfered with, then we can write

$$\underline{H} = \frac{\underline{H}_o}{\underline{J}}$$

For the tracker $\underline{J} = 1$ and the hypothesized $\underline{H}_o$ is the measured $\underline{H}$, which is shown in Figure 23. Assuming the simulator acts as a simple integrator ($\underline{J} = 1/j\ (\omega/\omega_o)$), the $\underline{H}$ for the simulator would be that shown in Figure 24. For comparison, the $\underline{H}$ actually measured in this case, on the simulator, is also shown in Figure 24. The value of ω_o used is that which makes the curves match. The equations solved by the simulator, however, reduce to a double integration ($\underline{J} = 1/(j\omega/\omega_o)^2$) at very low frequencies so that compensation of $\underline{H}$ for the characteristics of $\underline{J}$ seems incomplete. For an earlier reference to this sort of compensation, see page 70, reference 17.

As a further comparison of the two "transfer functions" in Figure 23, Figures 25 and 26 show the corresponding Nyquist diagrams. For the simple tracker, Figure 25, the necessary data for the Nyquist plot are just $\underline{H}$. For the case of the airplane aileron, the loop gain is $\underline{H}\,\underline{J}$, where for $\underline{J}$ we have used the approximation

$$\underline{J} = \frac{1}{j\left(\frac{\omega}{\omega_a}\right)^2 \left(1 + j\,\frac{\omega}{\omega_s}\right)}$$

where $\omega_a = 0.58$, and $\omega_s = 0.189$. This approximation is good up to $\omega = 4$. The constant ω_a appears as a gain, and therefore depends on the scale factors used in recording. For this reason it is slightly different than the $\underline{J}$ derivable from references (1) and (2).

Figure 25, the Nyquist loop for the simple tracker, is not distinguishable from the Nyquist diagrams plotted in reference (17) for the medium bandwidth case. See, for instance, Figures 11 and 12 of reference (17).

For Figure 26, the whole Nyquist diagram covers only the lower 1 rad/sec or so of the frequency scale. Variations, if any, in the amplitude of $\underline{H}$ have been fairly well smoothed out by the resolution bandwidth of the data reduction, although $\underline{H}$ is apparently a smooth function up to $\omega = 5$. Similarly the phase of $\underline{H}$ has been simplified by the approximation $\phi = 1.57 - 0.52\omega$, an expression which seems to agree with the experimental data within the accuracy of measurement over most of the measured frequency range. The assumption, then, is that the apparent smoothness of $\underline{H}$ over the computational range of frequencies is real, and that interpolations between data points are valid. Since the operator doesn't oscillate in flying the aircraft, the actual magnitude of the gain should provide more phase margin than Figure 26 indicates. A decrease of perhaps 25% would be reasonable. If this scale change is valid the Nyquist plot indicates that the operator has adjusted his parameters for just about optimal servo performance.

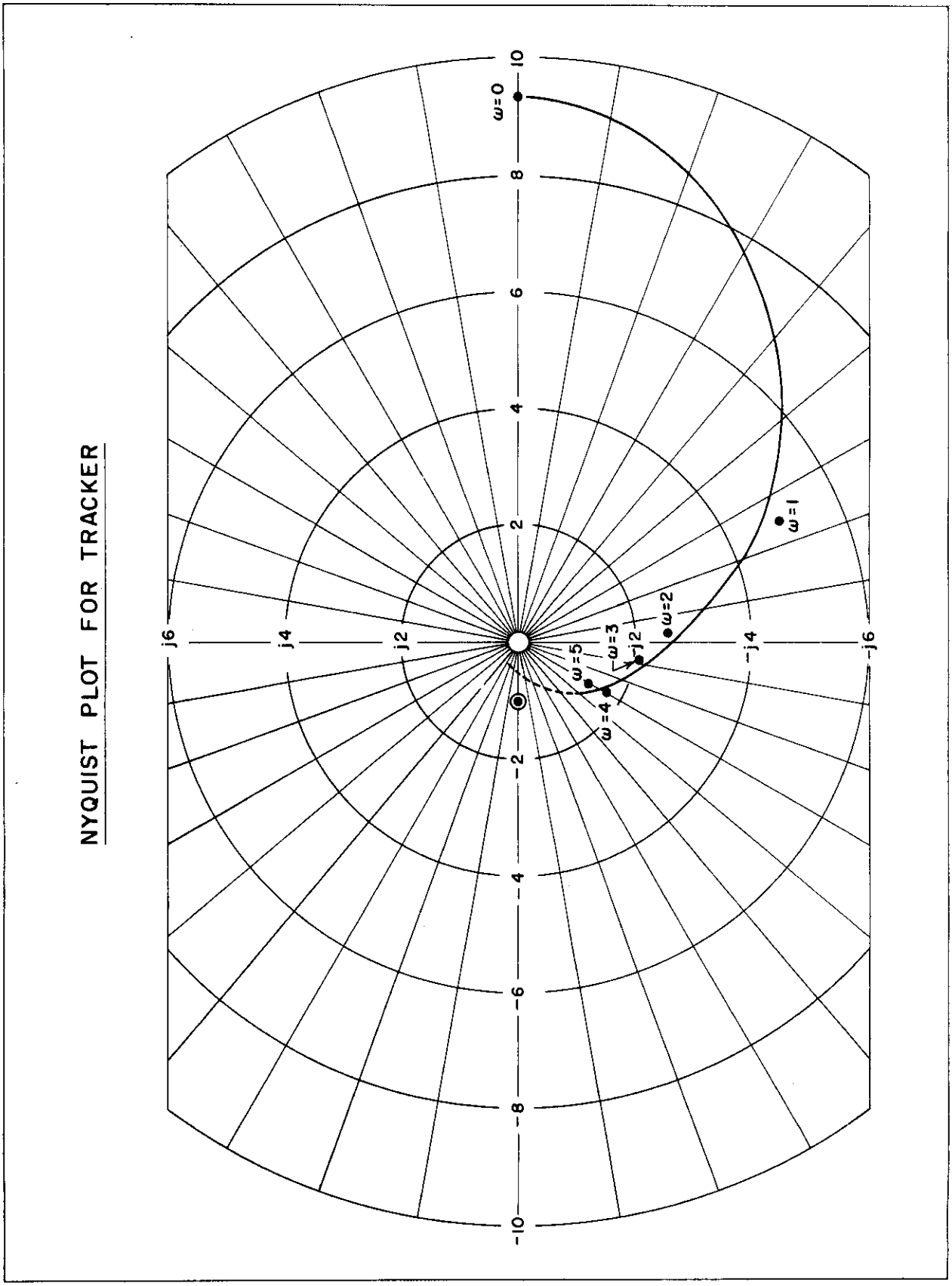

REPORT WADC TR 54-370

FIGURE 25

NYQUIST PLOT FOR AIRCRAFT SIMULATOR

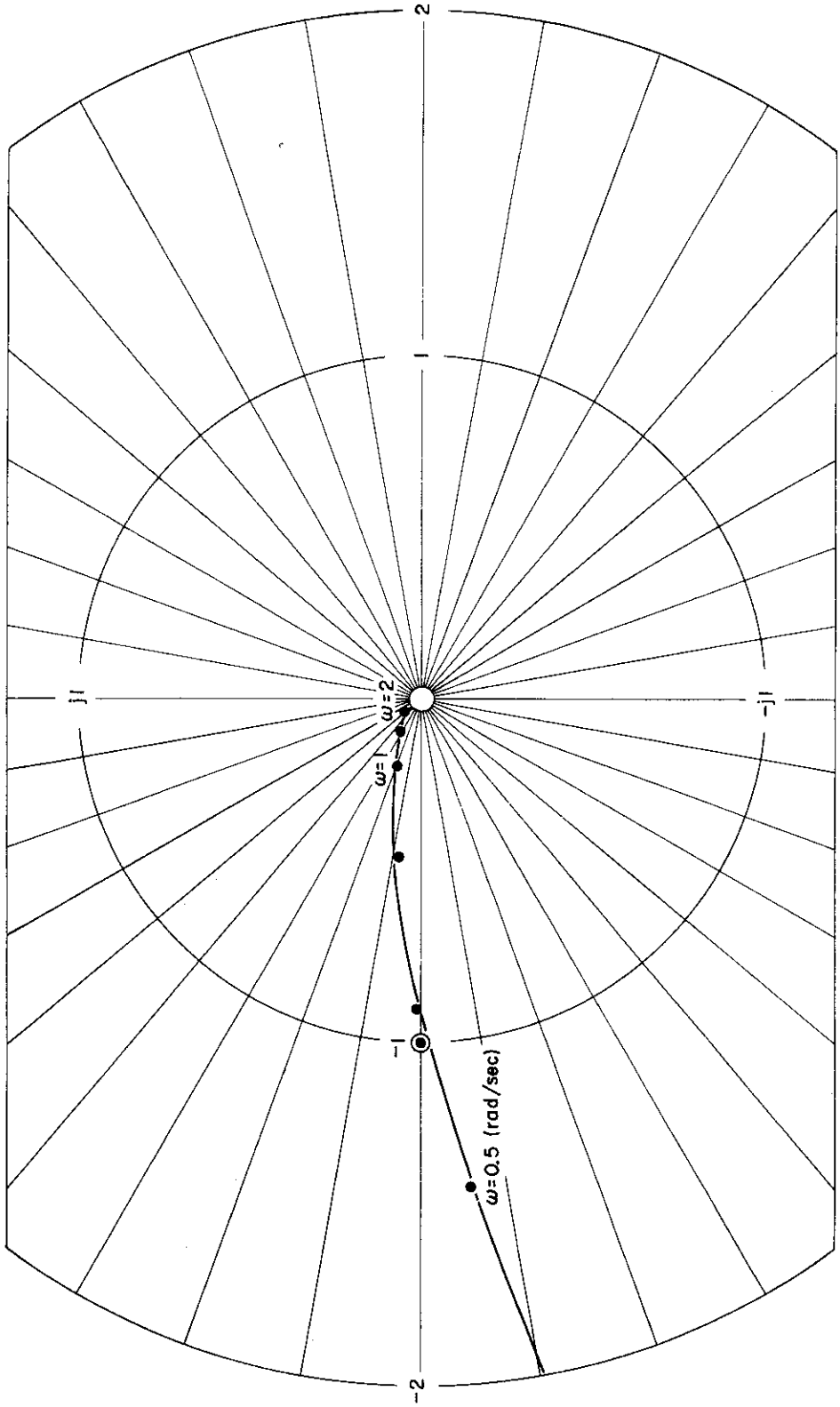

REPORT WADC TR 54-370

FIGURE 26

III. DISCUSSION

A. CONCLUSIONS

The problem toward which the work on this project is directed does not permit a simple answer. We are attempting to characterize mathematically the behavior of a complex operation, that of a pilot performing the difficult task of flying an aircraft. Our approach has been to assume that a usefully large part of this behavior may be described by a linear time invariant model derived from carefully specified measuring experiments. It then becomes an experimental problem to generalize this linear model. This means that we must determine the extent to which the model remains invariant as such parameters of the measuring experiments as input bandwidth amplitude, pilots, temporal factors, fatigue, habituation and so forth are changed. This is a long and involved process, but there is no alternative to it. The experiments in the section on results should be interpreted as part of this effort to generalize. Using the random input, as we do, we obtain what might be thought of as an expected "transfer function" averaged over a Gaussian amplitude distribution. Generalizing this "transfer function" essentially means performing further averaging procedures over pilots, over amplitude distributions of larger variances, over different types of aircraft, and, in fact, over all the parameters of this problem. Clearly, the central problem is to assign confidence limits to these expected or average "transfer functions", so that the usefulness of this characterization may be assessed. Thus, the goal of this research comes into sharper focus. We are searching for the expected value of a linearized "transfer function" to describe pilot responses together with a measure of the variance of this expected value. Furthermore, we are also interested in lawful trends. For instance, if as the pilot becomes fatigued perhaps his "transfer function" or the variance of his "transfer function" changes in a measurable manner with measurable fatigue; then both of these facts are important and deserve investigation.

For reasons previously elaborated, the results in Section III are fragmentary attempts at obtaining the expected "transfer function". The following conclusions may nevertheless be drawn from these results.

1. There are obvious differences in human "transfer functions" for different tracking tasks. These differences were measured in the tracker and in elevator and aileron control in the simulated aircraft. Actually, at this point, it would be well to reiterate the opinion that the analytical techniques which were applied to pilots can very usefully be applied to other pseudo-linear complicated control devices.

2. The evidence presented in the data indicates that day-to-day and trial-to-trial variations are quite small. An assumption of stationarity under the measuring conditions seems justified.

3. Phase characteristics for bandwidths 2 and 4 were sensibly the same. In both cases, the pilots exhibited average dead time lags of about 0.6 seconds for aileron control and 0.3 seconds for elevator control. In addition, from the limited evidence, the phase characteristics were only weakly, if at all, dependent on either pilots or forcing function amplitude.

4. Amplitude characteristics were not significantly affected by forcing function bandwidth. Pilots, and forcing function amplitude did, on occasion, cause significant differences in the amplitude response, as can be seen from the foregoing phase and amplitude curves.

5. Since this program has been at least partly inspired by the techniques of servoanalysis, a note on the Nyquist loci which could be plotted seems in order. In the tracker experiment, the gain reduces rapidly as the phase increases. In the airplane experiment, $\underline{J}$ drops off rapidly with frequency and includes phase lag. The pilot now may operate, and actually does operate, with higher gain at the higher frequencies, without violating the Nyquist criterion, and also seems to produce less phase lag.

6. Subject to flight test validation, and more extensive measurements, the enclosed data provide a first order approximation to pilot phase and amplitude characteristics in flying an F-80A. The reader should be careful of extrapolating the amplitude characteristics blindly because, of course, they will level off and fall at a frequency beyond our measuring range. Figures 11-14 represent reasonable estimates of pilot "transfer functions".

B. RECOMMENDATIONS

Much remains to be done.

1. The foregoing results must be studied for generalizability along the representative experimental variables mentioned previously. It is extremely important that the aircraft constants, which were parameters for the foregoing data, be made variables so that we can determine what sort of "transfer function" changes, if any, to expect in aircraft other than an F-80A flying a tail chase at 20,000 feet and Mach 0.7.

2. Flight tests should be conducted to investigate the extrapolation of ground simulator data to data gathered in the air.

3. This report is in no sense final. Many details remain to be filled in, i.e, additional Nyquist diagrams should be plotted, the confidence limits analysis should be made more rigorous, and so forth.

4. The data reduction apparatus, though operable, should be examined afresh with the view of making it more accurate, rapid, and less cumbersome.

BIBLIOGRAPHY

1. Glassman, I. A Dynamic Simulator for Study of Human Response Characteristics. Transactions of the IRE Professional Group on Airborne Electronics. October 1952.

2. Deily, W. H., Glassman, I. and Houghton, D. B. A Dynamic Aircraft Simulator for Study of Human Response Characteristics - Franklin Institute Report F-2169. AF 33(038)-10420. September 1952.

3. Barnes, G. H. Data Reduction Equipment for the Analysis of Human Tracking. Franklin Institute Report F-2333. AF 33(616)-270. May 1953.

4. Krendel, E. S. Suggested Preliminary Use of the F-80 Dynamic Simulator. Franklin Institute Working Paper Al 2169-4. January 22, 1952.

5. Krendel, E. S. Addendum to Working Paper No. 1 of January 22, 1952, 2169-4, Franklin Institute. April 4, 1952.

6. Krendel, E. S. On Computing Descriptive Functions. Franklin Institute Working Paper No. 1, 2333-1. September 25, 1952.

7. Krendel, E. S. Background for the First Experiment Using the Dynamic Aircraft Simulator and Harmonic Analysis Data Reduction. Franklin Institute Working Paper No. 1, 2169-6. January 6, 1953.

8. Krendel, E. S. Outline of the Second Experiment. Franklin Institute Working Paper No. 2, 2169-6. January 21, 1953.

9. Krendel, E. S. Experiment Three: Input Amplitude Effects. Franklin Institute Working Paper No. 3, 2169-6. February 13, 1953.

10. Krendel, E. S. Information Theory and Tracking. Franklin Institute Working Paper No. 4, 2169-6. March 23, 1953.

11. Krendel, E. S. Report On the Use of the Dynamic Simulator. Franklin Institute Report I-2169-2. AF 33(038)-10420. July 1952.

12. Krendel, E. S. A Preliminary Study of the Power Spectrum Approach to the Analysis of Perceptual Motor Performance. AF TR No. 6723, WADC. October 1951.

13. Krendel, E. S. The Spectral Density Study of Tracking Performance; Part 1. The Effect of Instructions. WADC TR 52-11 Part 1, WADC. January 1952.

14. Krendel, E. S. The Spectral Density Study of Tracking Performance; Part 2. The Effects of Input Amplitude and Practice. WADC TR 52-11 Part 2, WADC. January 1952.

15. James, H. M., Nichols, N. B. and Phillips, R. S. Theory of Servomechanisms. McGraw-Hill 1947. pp 278-279.

16. Elkind, J. I. Tracking Response Characteristics of the Human Operator. HFORL Memorandum No. 40. September 1953.

17. Russell, L. Characteristics of the Human as a Linear Servo-Element. Servomechanisms Laboratory, MIT. May 1951.

18. Arthur, G. R. A Note on the Approach of Narrow Band Noise after A Non-Linear Device to a Normal Probability Density. J. Appl. Phys. Vol. 23. 1952. pp 1143-44.

19. Tukey, J. W. On Sampling Theory of Power Spectrum Estimates. Symposium on Application of Autocorrelation Analysis to Physical Problems, ONR. 13-14 June 1949. pp 47-67.

20. Blackman, R. B. Introduction to Spectra of Time Series. Bell Telephone Laboratories. August 1951.

21. Spetner, L. M. Errors in Power Spectra Due to Finite Sample. J. Appl. Physics. Vol. 25, 1954. pp 653-659.

22. Bartlett, M. S. Periodogram Analysis and Continuous Spectra. Biometrika. Vol. 37. 1950. pp 1-16.

23. Tukey, J. W. Measuring Noise Color. Bell Telephone Laboratories. 1951. p. 28.

24. Krendel, E. S. A Survey of Suggested Mathematical Models for the Study of Human Pilot's Responses. Second Piloted Aircraft Flight Control System Symposium, Bu Aer Report AE-61-5-III. June 1951. pp. 128-135.

IV. APPENDIX I

NOISE SOURCE

The requirements on the noise source are that it have two independent outputs, both of them variable in bandwidth and amplitude with bandwidths of the order of a few radians per second. One, two, and four radians per second were chosen for the bandwidths. The other requirement is that the output spectrum be essentially flat at the low frequency end, down to a twentieth or a thirtieth of a cycle per second.

The method chosen involves the following steps: generation of the broad-band gas tube noise, sampling of this noise at a fairly high rate (several hundred cycles per second), and preservation of these samples with a storage condenser. This would yield noise like that of Figure 1a, with a spectrum which is flat well past the desired noise bandwidth. This noise is then low-pass filtered to get the final output. The wave-form in the equipment actually contains a sawtooth carrier component as in Figure 27, but this is irrelevant, being removed by the low-pass filtering.

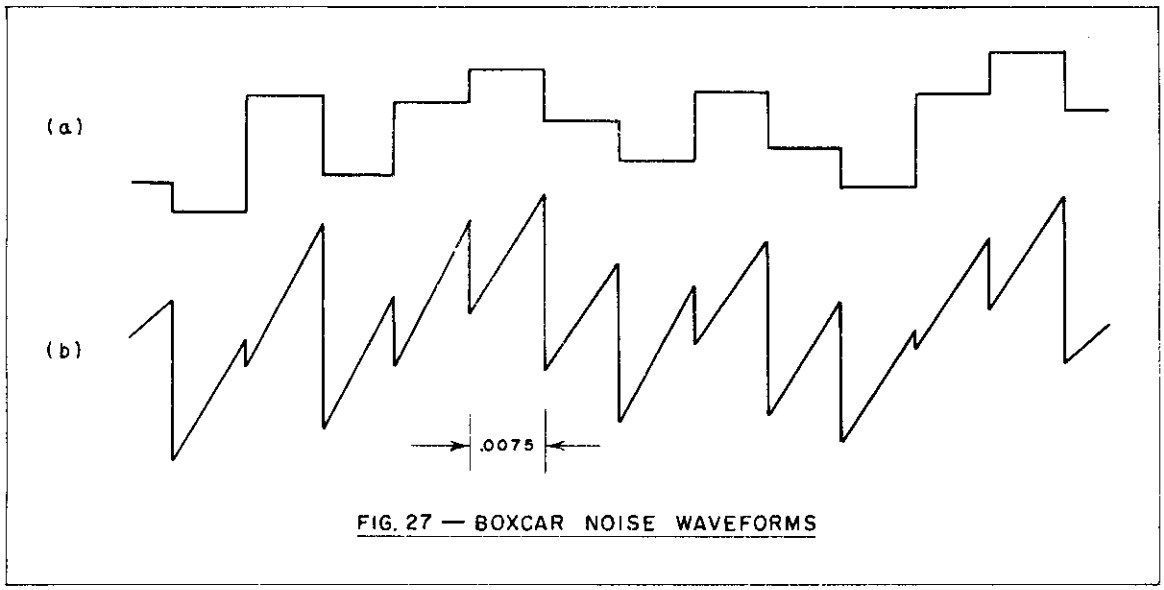

FIG. 27 — BOXCAR NOISE WAVEFORMS

To simplify the circuits, both output channels of noise (x and y), come from the same gas-tube noise source. The samples are alternately taken first from one channel and then from the other, with time enough between so that they are independent. The filter circuits are duplicated. The block diagram of the equipment just described is shown in Figure 28. To remove any d-c level in

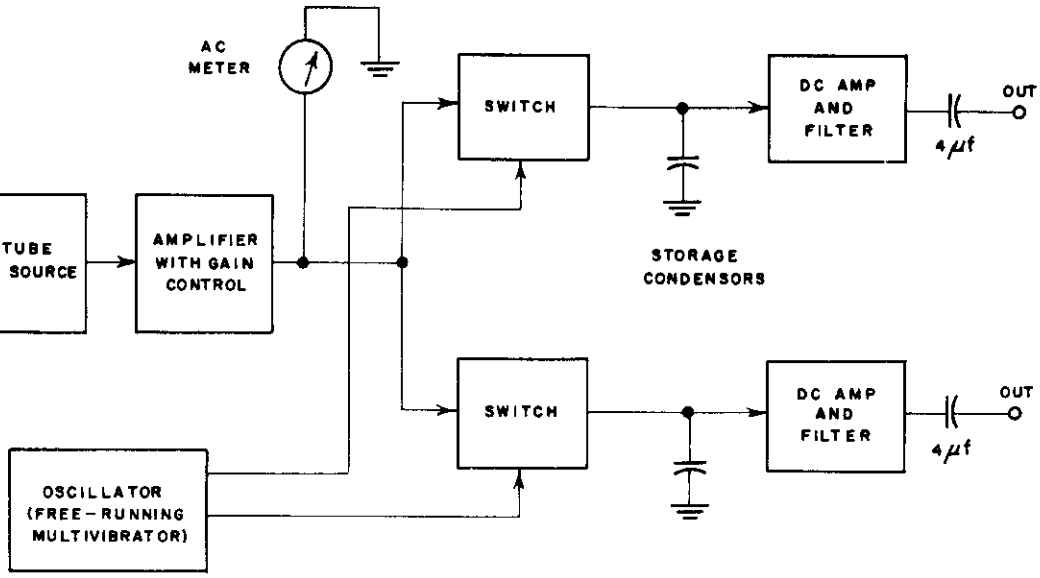

FIG. 28 — NOISE SOURCE BLOCK DIAGRAM

the output, a large blocking condenser is included. This is intended to work into a one megohm load, so that the low frequency cut-off is at one twenty-fifth of a cycle per second. A cathode follower is also provided to furnish a low impedance output for recording purposes.

The low-pass filtering is done with three cascaded stages of RC filtering, such that the output power spectrum is given approximately by

$$\bar{\Phi}(\omega) = \frac{\frac{A}{\omega_o}}{\left[1 + \left(\frac{\omega}{\omega_o}\right)^2\right]^3} \qquad (29)$$

ω_o takes on the values 1, 2, and 4, and the magnitude A is controlled both by a gain control in the amplifier after the gas tube, and by a step attenuator in the output amplifier giving 0, 6, and 12 d.b. of attenuation. The factor $1/\omega_o$ in equation (29) was introduced to hold rms power constant as bandwidth is varied.

The final circuit diagram is given in Figure 29. The unit was built on one 5 1/4" rack-mounted panel.

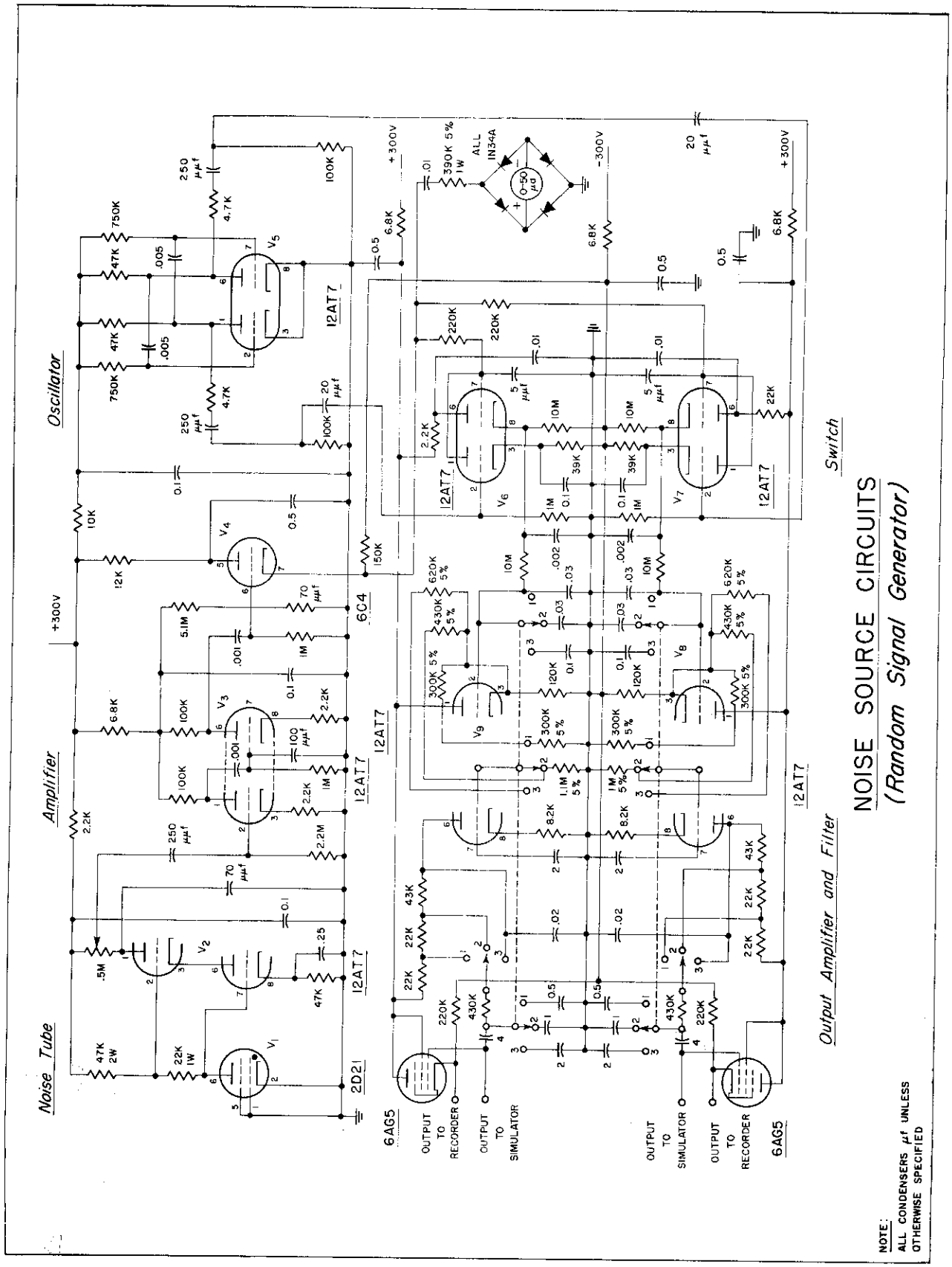

REPORT WADC TR 54-370

FIGURE 29

V. APPENDIX II

DATA REDUCTION APPARATUS; COMPUTATIONAL AND PROCEDURAL DETAILS

Although the data reduction apparatus has been discussed in a previous final report (Ref. 3), there is value in restating some of the discussion in this appendix. In addition, certain modifications in the computing procedure which have not previously been a detailed matter of record, will be stated.

The method of computation which is outlined in equations listed under Reference (1) was proposed by Dr. J. W. Tukey in an informal conversation with the author.

Consider two time functions c(t) and f(t), which represent the control response of the pilot and the forcing function input to the aircraft respectively. Furthermore, consider circuitry capable of phase-shifting all the Fourier components of one of the time signals by 90°. This new function may be denoted by $f(t)_{90^\circ}$. One can form all of the possible sums and differences, involving both input and output, of the aforementioned three time signals. On computing the power spectra, denoted by P[ ], of these sums and differences, the following results. The Co and Qua terms referring to copower and quadrature power are introduced for convenience in subsequent manipulation. As in the body of the report $\bar{\Phi} \equiv \bar{\Phi}(\omega)$.

$$
\begin{aligned}
C_o^{+} &\equiv P[f(t) + c(t)] = \bar{\Phi}_{FF} + \bar{\Phi}_{CC} + 2R_e\{\bar{\Phi}_{FC}\} \\
C_o^{-} &\equiv P[f(t) - c(t)] = \bar{\Phi}_{FF} + \bar{\Phi}_{CC} - 2R\{\bar{\Phi}_{FC}\} \\
Qua^{+} &\equiv P[f(t) + c(t)_{90^\circ}] = \bar{\Phi}_{FF} + \bar{\Phi}_{CC} + 2I_m\{\bar{\Phi}_{FC}\} \\
Qua^{-} &\equiv P[f(t) - c(t)_{90^\circ}] = \bar{\Phi}_{FF} + \bar{\Phi}_{CC} - 2I_m\{\bar{\Phi}_{FC}\}
\end{aligned}
\qquad (30)
$$

The foregoing equations (30) can be derived rather simply by working from the autocorrelations of the sums and differences.

The function which we want to compute is $\bar{\Phi}_{FC}$, a complex function.

$$\bar{\Phi}_{FC} \equiv R_e\{\bar{\Phi}_{FC}\} + jI_m\{\bar{\Phi}_{FC}\} \qquad (31)$$

From equation (30)

$$\bar{\Phi}_{FC} = \frac{1}{4}\{[Co^{+} - Co^{-}] + j[Qua^{+} - Qua^{-}]\} \qquad (32)$$

The data reduction apparatus produces outputs measuring the square roots of Co^+, Co^-, Qua^+ and Qua^-. This use of a linear rather than a square law detector is open to criticism. The arguments justifying the use of a linear detector are summarized below.

If W(x) is the probability distribution of amplitudes in the input signal, the output of a linear detector may be written as follows:

$$E_L = \int_0^\infty x\ W(x)\ dx$$

Similarly the output of a quadratic detector may be written as

$$E_q = \int_0^\infty x^2\ W(x)\ dx.$$

It follows that $E_q = KE_L^2$ where the constant K depends only on the form of the probability density W(x). In this particular problem, the input to the detector comes from a narrow band filter. A heurustic argument based on the central limit theorem may be used to convince one's self that the output of a narrow band filter is Gaussian when the input is any time-stationary noise, Gaussian or not(18). However, J. W. Tukey has pointed out in private correspondence to the author that it does not follow that the output will be Gaussian in general. Be this as it may, it is reasonable to expect that K will be essentially a constant for almost all of our records. In addition K is not a strong function of the form of W(x). The foregoing arguments tend to indicate that variations in local average power must be rather strong before K changes to such an extent that our results are not meaningful. The Gaussian noise inputs to the simulator do not exhibit such a variation. If the pilots exhibit such a variation, this is a strong indication of expressively non-linear behavior on the part of the pilot, and we should in this case figure out a different, non-linear technique for analyzing the data.

In a continuation of a correspondence on this matter, J. W.Tukey agreed that for a problem of uniform difficulty the foregoing argument on the equivalence of the two means of detection was valid. If, however, the difficulty of the task varies over the loop, then the detectors are not equivalent. So much for this aside.

In brief, the data reduction apparatus works as follows. The time signals e(t), c(t), and f(t), previously described in this report, are recorded on tape transported at the rate of 1-3/4 inches per second. These recordings are time series samples of two minute's duration which after being suitably smoothed at the beginning and end of the run, are spliced to form endless loops. The loops are played back at 60 in./sec into a wave analyzer and the amplitudes of interest are measured on a recording milliameter. The details of the foregoing process are described in (3). Several changes, however, have taken place in the mechanical procedures outlined in the referenced report.

A modulation scheme about 120 cps as center frequency was used in an effort to get greater detail at low frequencies than was possible in the scheme described in (3). The frequencies of interest are translated to the region above and below 120 cps. since the wave analyzer does not go below 20 cps in its response. The suppressed-carrier system used eliminates all limitations on the low frequency response of the analyzer except those inherent in the resolution conditions which follow from sample length. Since our resolution is approximately one radian, we can now compute a point at 0.5 radians by averaging the band of frequencies extending from zero to one radian.

Instead of mechanically scanning the dial on the wave analyzer and thus obtaining a continuous spectrum, as was originally planned, a series of discrete measurements were made. Figure 30 shows a sample record. The wave analyzer dial was set in discrete five cps steps from 90 to 140 cps. At each frequency setting the following were measured: the quantities Co^-, Co^+, Qua^-, and Qua^+ for $\bar{\phi}_{CF}$ and for $\bar{\phi}_{EF}$ and the power spectra for e(t), c(t), and f(t). In all, eleven numbers were obtained for each fixed frequency setting. In effect the continuous frequency scale was being digitalized. The purpose for this action was that previous computations based on continuous recordings were meaningless due to a high computing noise level. In the computations it is necessary to add and to divide terms computed at a given frequency. The wave analyzer settings for given frequencies were not absolutely stable from run to run; hence errors arose because frequencies were not accurately comparable across runs. It turned out that much better results were obtained when the aforementioned computations were all made at the same fixed frequency, even though this fixed frequency differed from the wave analyzer nominal frequency by some small amount.

Actually, it should not have been necessary to measure the spectral values over the range of 90 to 140 cps, (a range corresponding to almost ten radians in tracking bandwidth) since the data were either symmetrical or antisymmetrical about the modulation frequency. It was useful, however, to perform this extra work for the following reasons. Dial readings were not strictly comparable, but in all cases an inter-curve-comparable zero frequency point could be obtained from the axis of symmetry or antisymmetry. In addition, the fact that reduced data must be symmetrical or antisymmetrical (depending on whether real or imaginary parts of the cross spectra were being computed)gives us a quick method for determining whether the data reduction apparatus was working properly. Figures 31 and 32 illustrate data which met the symmetry and anti-symmetry requirements. Note that $\bar{\phi}_{CF}$ and $\bar{\phi}_{EF}$ are antisymmetrical. The amplitude data, however, are symmetrical. The symmetry conditions are necessary but not sufficient for valid data. In the final results the symmetrical and antisymmetrical points were averaged together for each individual record after the reflections about the axis of symmetry had been properly made.

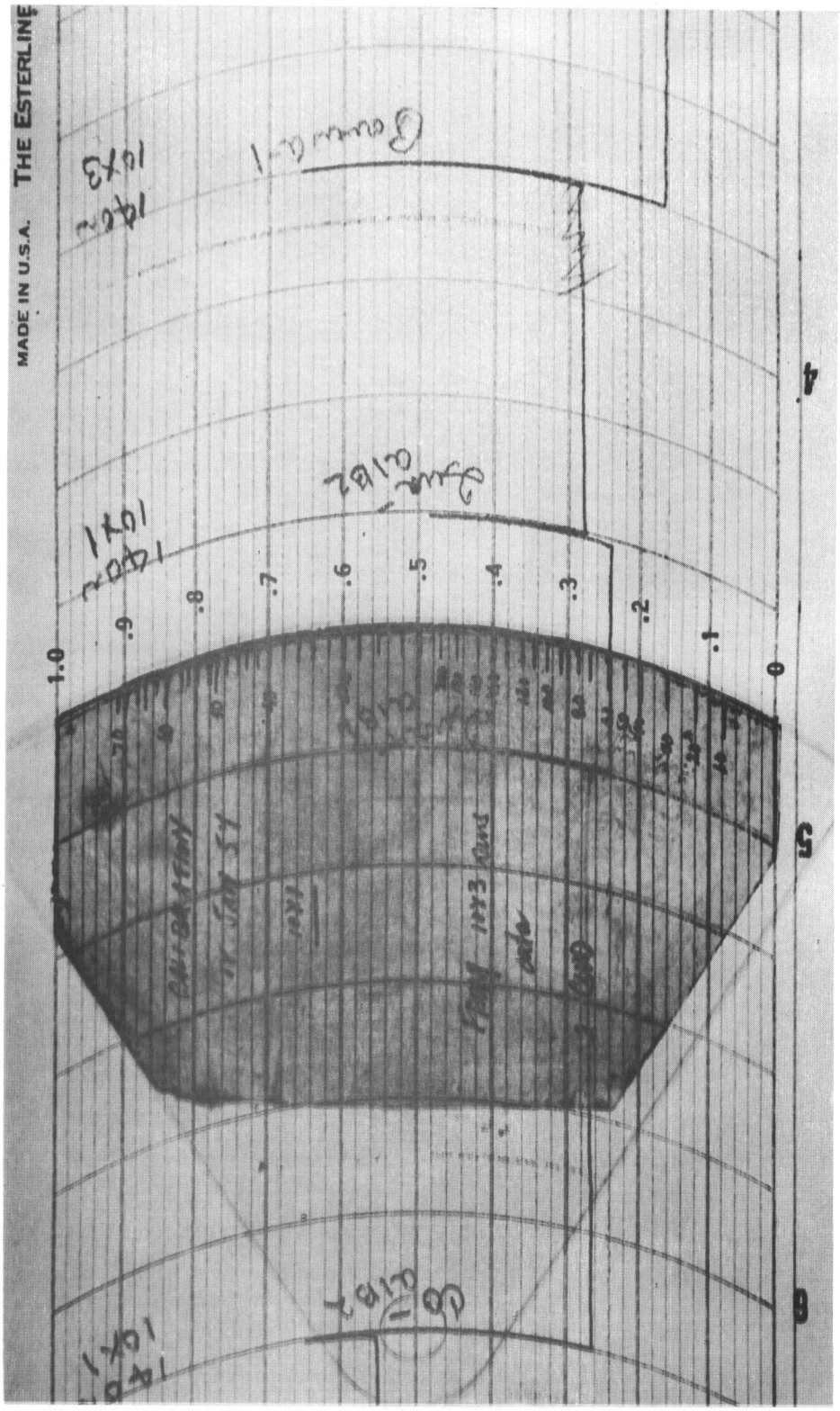

A SAMPLE RECORD

CROSS SPECTRA FOR AILERON RESPONSE

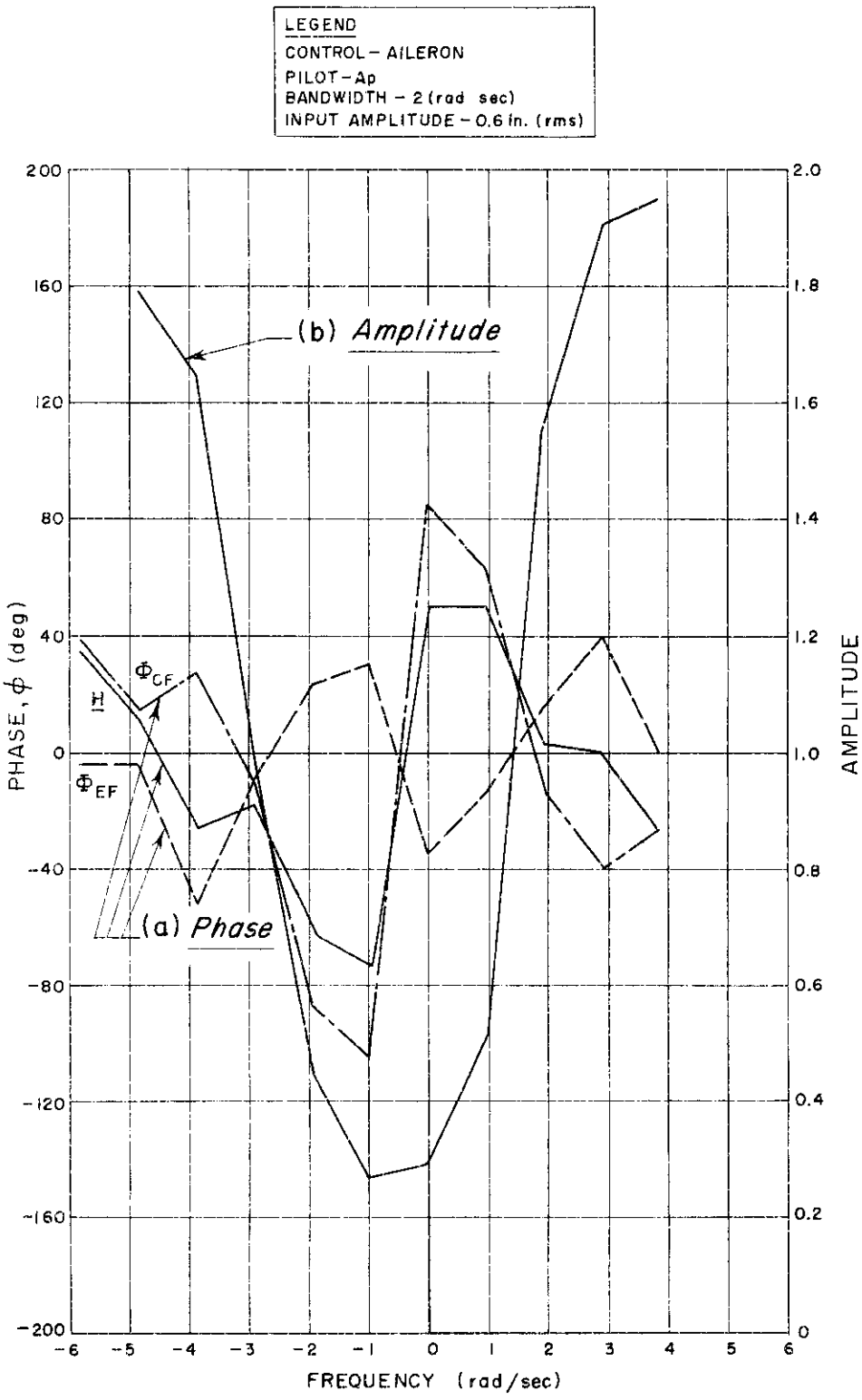

REPORT WADC TR 54-370

FIGURE 31

CROSS SPECTRA FOR ELEVATOR RESPONSE

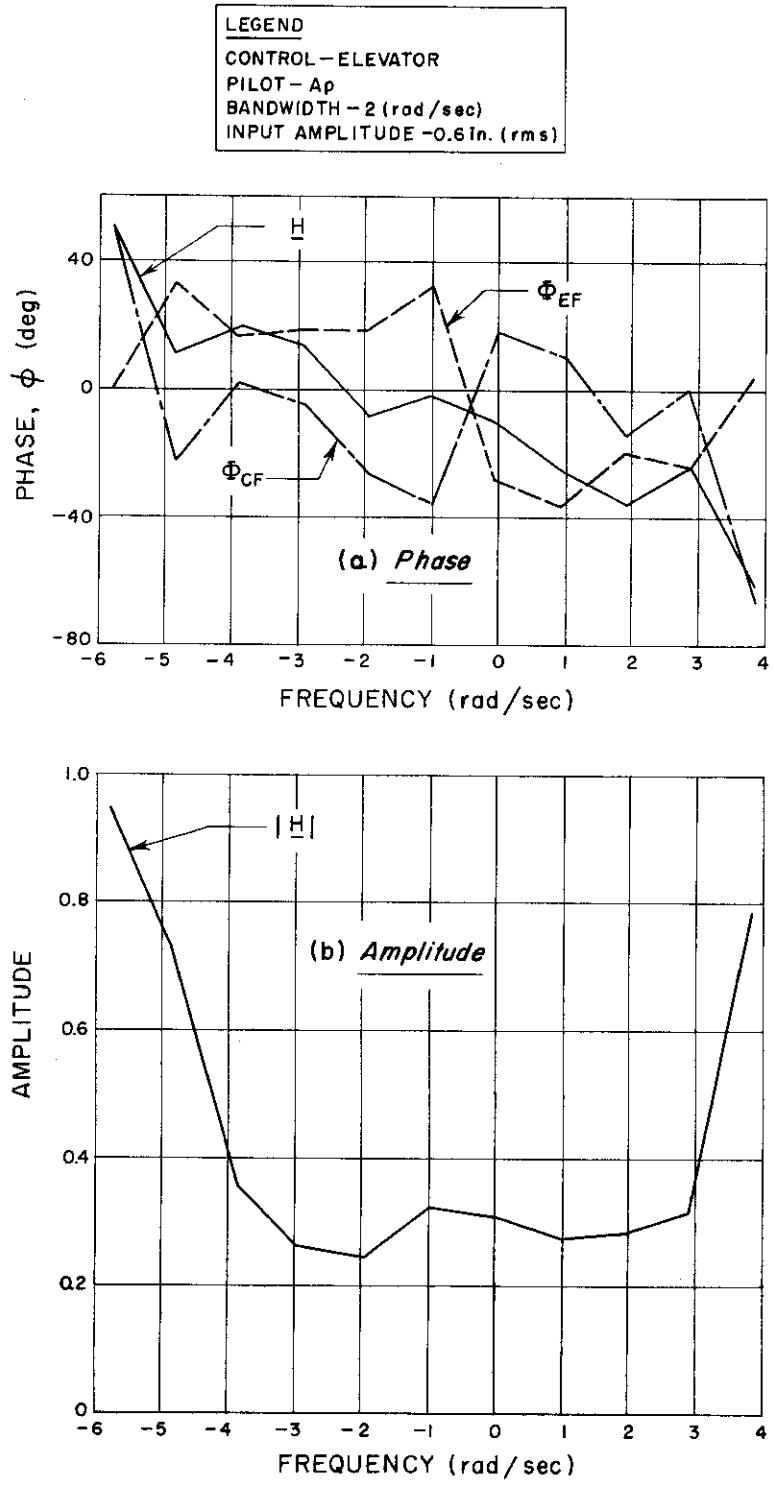

REPORT WADC TR 54-370

FIGURE 32

One last modification was dictated by a basic difficulty with the data reduction procedure. In general, the entire cumbersome set of computations, which will be outlined further along, had to be carried out before it was possible to tell whether or not the apparatus was computing properly. Several attempts were made to set up a check procedure. For example, a passive network of known transfer function was used as a basis for a check procedure. Figure 33 shows the comparison between the theoretical transfer function for this network and the transfer function measured up to an input signal attenuation of 60 db. Gratifying as this result was, it did not provide a simple check that could be made rapidly at frequent intervals while the tape was being played back. After some difficult trouble shooting it was discovered that much of the data reduction difficulties were due to either dirt or magnetic compound rubbing off of the tape and filling up the microscopic air gaps in the heads. (It would have been far better, indeed, from this viewpoint were copper gaps used in the heads.) When the heads became "loaded" the signal level would drop, and the fm discriminators would operate from amplifier noise instead of the desired signal. An aural monitor was designed so that this "loading" of the playback heads could be detected before erroneous measurements were made. The cure for this problem was, in cases of mild loading, to flick the tape, thus dislodging the matter; or, in bad loading, to stop operations and clean the heads with ethyl alcohol.

The computational procedures required after the various discrete output data had been recorded were as follows. A nomograph reading device, which may be seen overlaying the raw data in Figure 30, was used to simultaneously convert the signal levels to voltages and to square these voltages. The nomograph values were obtained by an input output calibration of the data reduction apparatus.

The data for Co^-, Co^+, Qua^-, Qua^+ and $\overline{\Phi}_{11}$ thus obtained, were manipulated as follows. As dictated by equation (30)

$$\frac{1}{4}(Co^+ - Co^-) = R_e\{\overline{\Phi}_{FC}\} \tag{26}$$

and

$$\frac{1}{4}(Qua^+ - Qua^-) = I_m\{\overline{\Phi}_{FC}\}$$

were computed. The real and imaginary parts were combined in the usual manner to obtain the magnitude and phase for

$$\overline{\Phi}_{FC} = M(\omega)\ e^{j\phi_1} \tag{27}$$

THEORETICAL AND MEASURED TRANSFER FUNCTION OF A PASSIVE NETWORK

(Measured by an Input of One rad/sec Bandwidth)

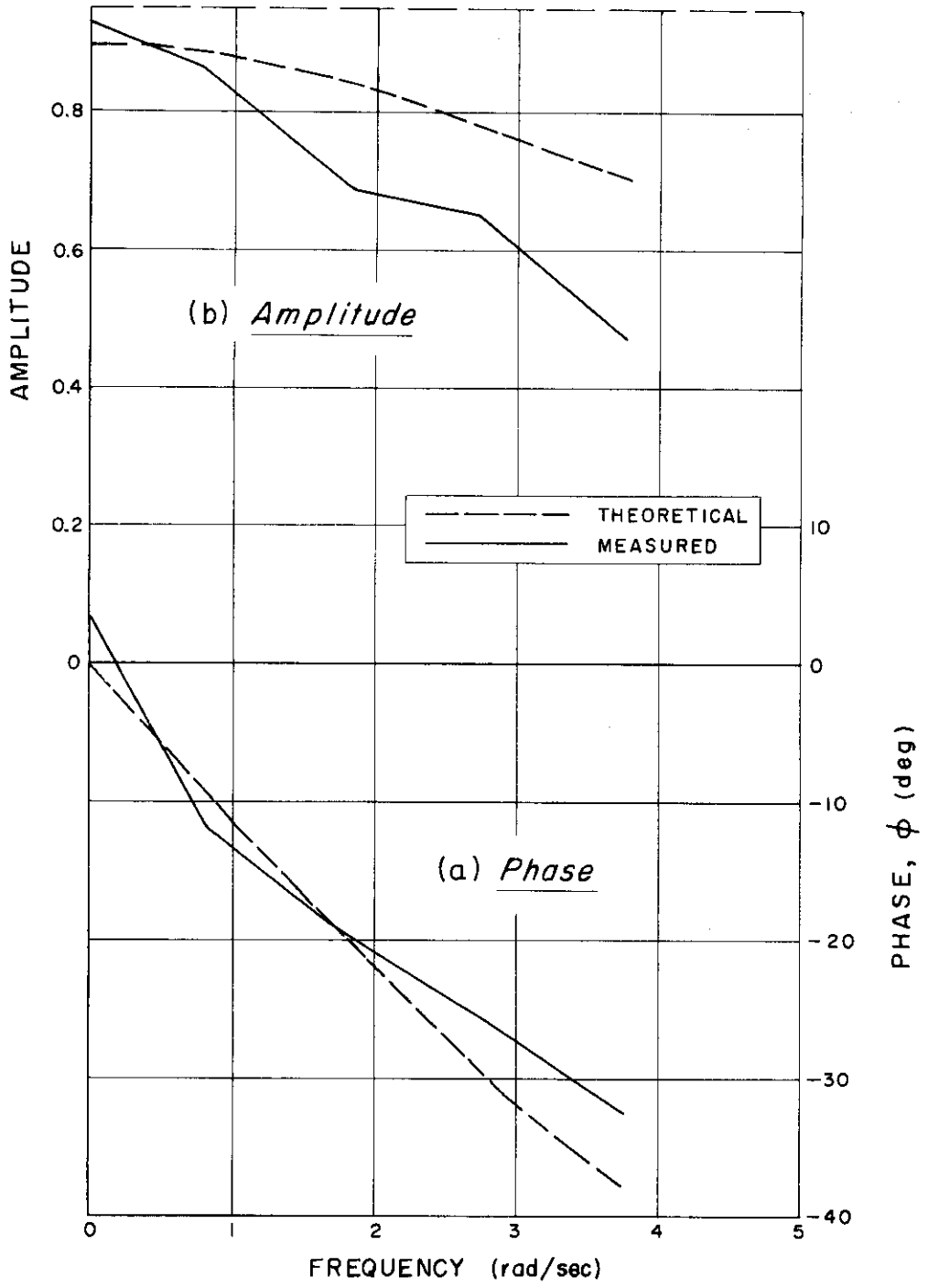

REPORT WADC TR 54-370

FIGURE 33

$$M(\omega) = [R_e^2\{\bar{\Phi}_{CF}\} + I_m^2\{\bar{\Phi}_{CF}\}]^{\frac{1}{2}}$$

$$\phi = \arctan \frac{I_m\{\bar{\Phi}_{CF}\}}{R_e\{\bar{\Phi}_{CF}\}} \qquad (28)$$

An analogous computation was carried out for $\bar{\Phi}_{EF}$. The phase responses for both $\bar{\Phi}_{EF}$ and $\bar{\Phi}_{CF}$ were plotted, for both negative and positive frequencies, upon the same paper. The difference between these curves, with careful attention to 180° phase changes in the apparatus, denotes the phase characteristic corresponding to equation(11) in the body of the report.

Figures 34 and 35 are the data which when averaged become Figures 11a and 11b in the body of this report. Figures 34 and 35 illustrate the variability from repeat performance to repeat performance by the same subject.

It might be noted that constant reaction type lags can be extracted from either the difference or the individual phase responses by merely computing the derivatives of the straight portions of the curves. This follows from the fact that a constant delay of time, T, would be expressed as $e^{j\omega T}$ and the derivative of the phase angle is simply T. Figures 36 and 37 are tracking record data for $\bar{\Phi}_{CF}$. Note the fixed lag implied by the constant slope.

The attenuation or gain for equation (11) is simply $|\bar{\Phi}_{CF}|$ divided by $|\bar{\Phi}_{EF}|$.

"TRANSFER FUNCTIONS" BEFORE AVERAGING, Phase

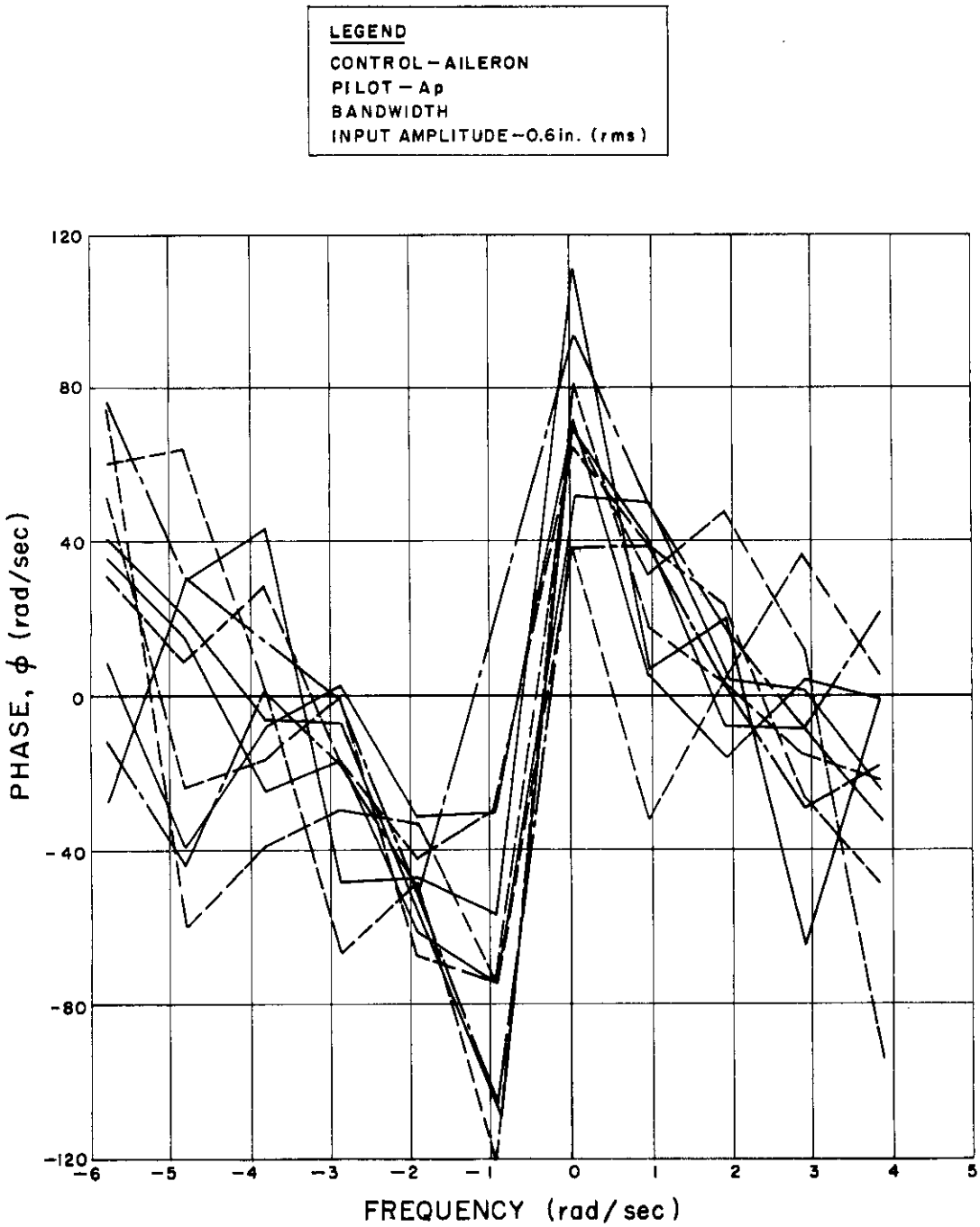

REPORT WADC TR 54-370

FIGURE 34

"TRANSFER FUNCTIONS" BEFORE AVERAGING, Amplitude

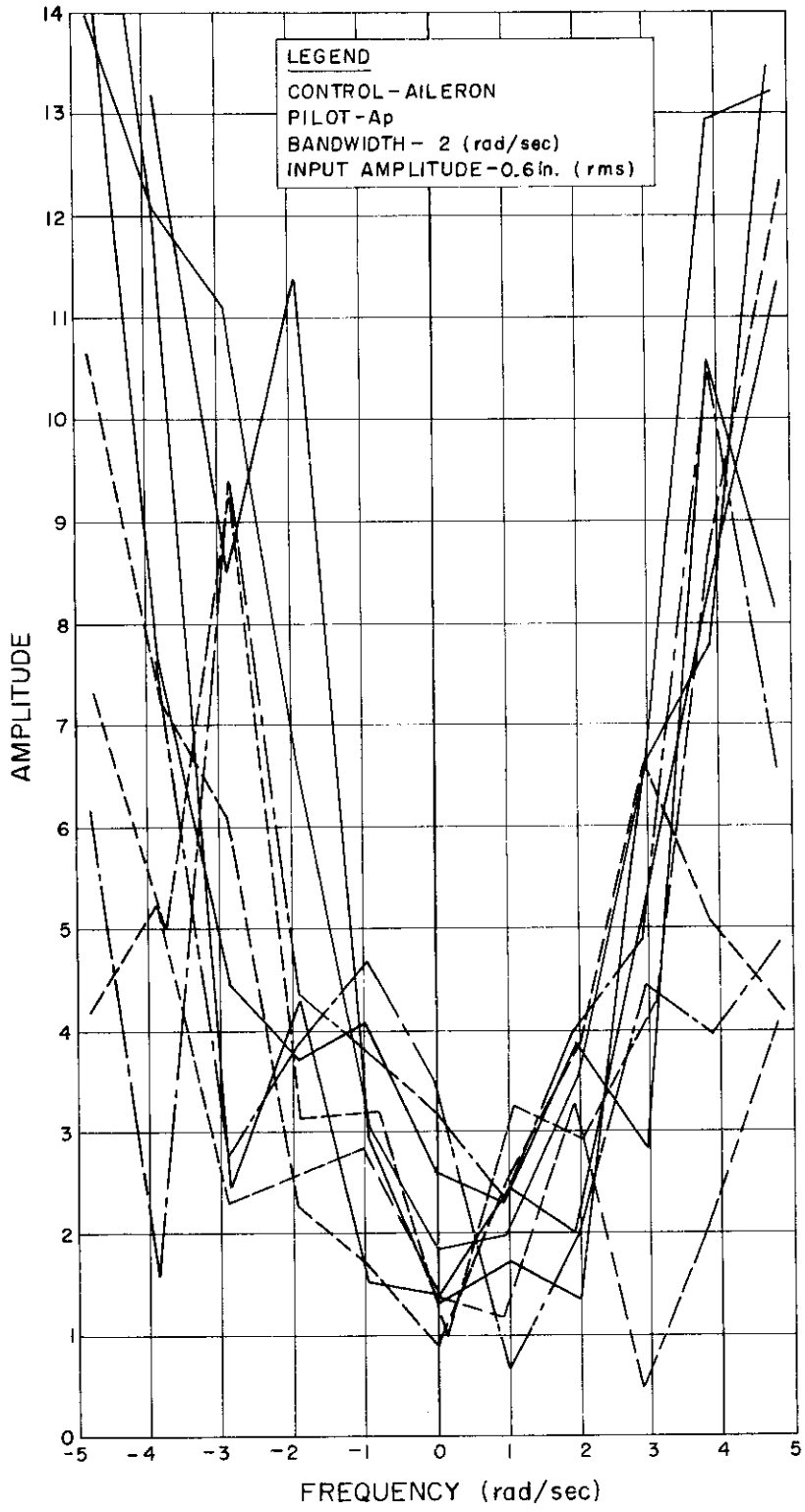

REPORT WADC TR 54-370

FIGURE 35

CROSS SPECTRA FOR SIMPLE TRACKER, PHASE, 2 (rad/sec)

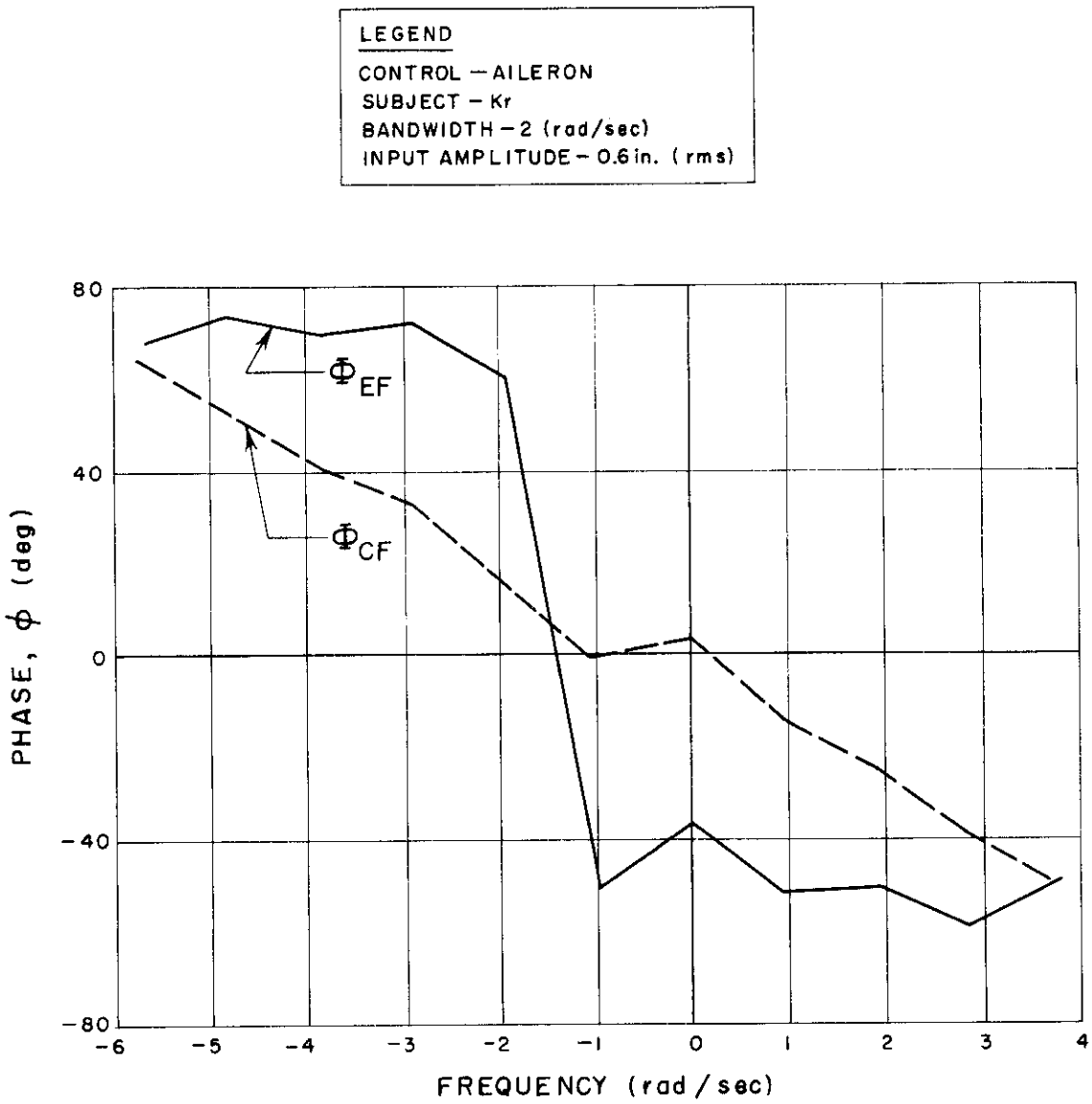

REPORT WADC TR 54-370

FIGURE 36

CROSS SPECTRA FOR SIMPLE TRACKER, PHASE, 4 (rad/sec)

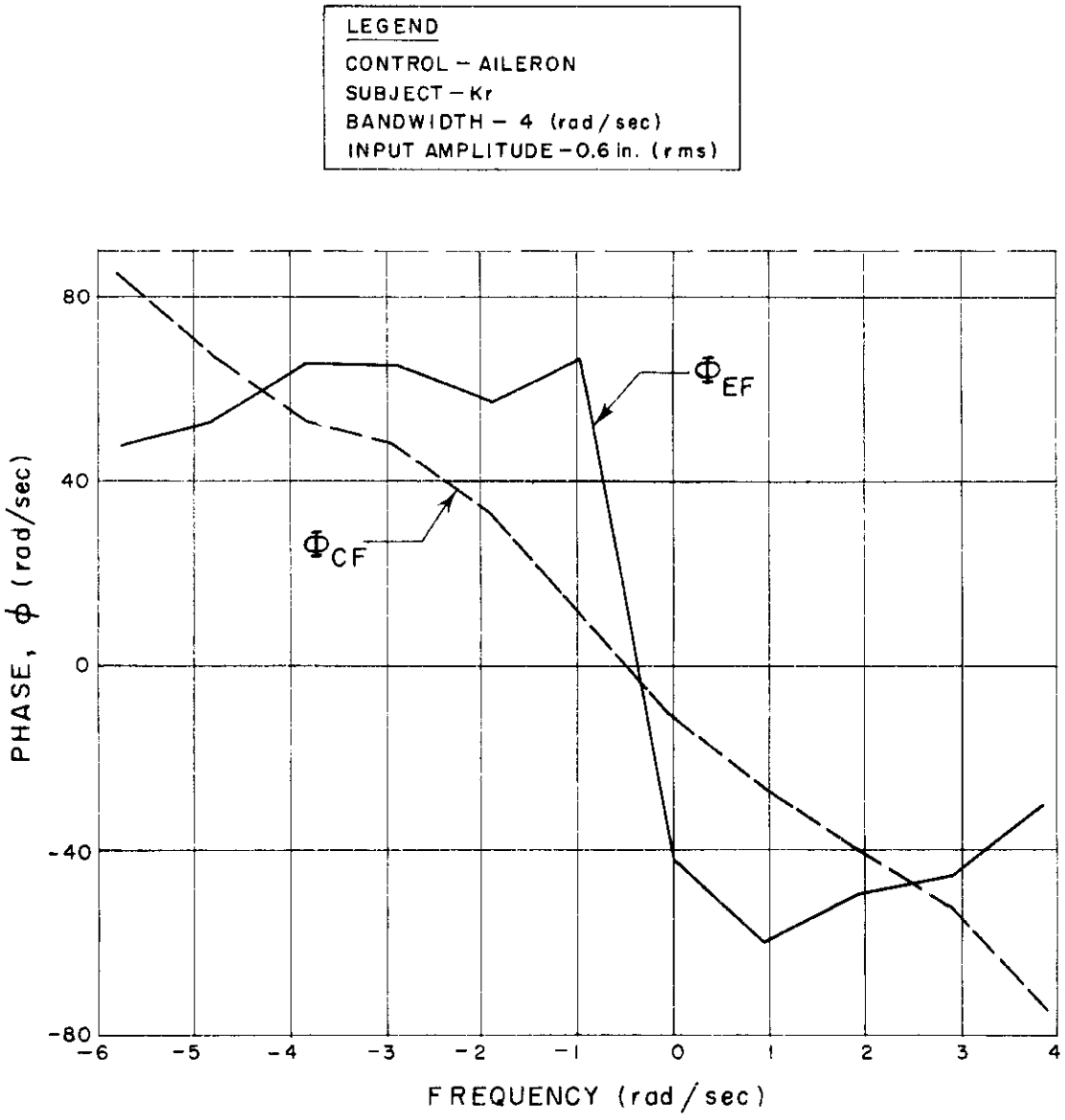

REPORT WADC TR 54-370

FIGURE 37

VI. APPENDIX III

CONFIDENCE LIMITS

The end results of the measurement program described in this report are a series of phase and amplitude characteristics obtained by following a rather complicated computational procedure. It is necessary to have some estimate of accuracy with which these characteristics are known. This appendix presents a quick attempt to assign confidence limits to the end results.

The total confidence limit assigned to a measurement will be composed of both sampling and computer noise variance. The propagation of these two types of errors will be considered separately and two variances will be combined at the end of this development.

Let us first consider sampling errors. The general approach will be to express the descriptive function or pseudo "transfer function", $\underline{H}$, which is calculated, as a function of three independent Gaussian noises F, N and P, defined in the body of this report. Then, the calculated $\underline{H}$ will be expressed as the sum of the true $\underline{H}$, $\underline{H}_T$, plus first order error terms. The distribution parameters for these error terms will then be computed and it will be shown how these parameters affect the phase and amplitude characteristics.

Following equation (9) in the body of this report

$$\underline{H} = \frac{\underline{\Phi}_{CF}}{\underline{\Phi}_{EF}} = \frac{(\overline{NF^*} + \underline{H}_T\overline{FF^*} - \underline{H}_T\overline{PF^*})}{(\overline{FF^*} - \underline{J}\,\overline{NF^*} - \overline{PF^*})} \tag{33}$$

Throughout this appendix, $\underline{H}$ unsubscripted means calculated $\underline{H}$. Using the usual symbol, <>, for ensemble average to denote the true value for the above averages one can write the calculated time averages as true averages plus small errors.

$$\overline{FF^*} = \langle FF^* \rangle + \epsilon_{FF} = \Phi_{FF} + \epsilon_{FF} \tag{34}$$

$$\overline{NF^*} = \langle NF^* \rangle + e^{j\phi_1}\epsilon_{NN} = 0 + e^{j\phi_1}\epsilon_{NF}$$

$$\overline{PF^*} = \langle PF^* \rangle + e^{j\phi_2}\epsilon_{PF} = 0 + e^{j\phi_2}\epsilon_{PF}$$

In the above, ϵ_{FF} is a real quantity, but the errors associated with the complex cross spectral estimates have imaginary components. Equations (34) may now be substituted into (33) in order to relate the calculated $\underline{H}$ to $\underline{H}_T$. In evaluating the eventual expressions for the error, we will be forced to use $\underline{H}$ calculated as our best and only estimate of H_T. This will cause a negligible error in our heuristic treatment.

$$\underline{H} = \frac{(e^{j\phi_1}\,\epsilon_{NF} + \underline{H}_T[\underline{\Phi}_{FF} + \epsilon_{FF}] - \underline{H}_T\, e^{j\phi_2}\,\epsilon_{PF})}{(\underline{\Phi}_{FF} + \epsilon_{FF} - \underline{J}\, e^{j\phi_1}\,\epsilon_{NF} - e^{j\phi_2}\,\epsilon_{PF})} \tag{35}$$

$$\underline{H} = \frac{\underline{H}_T\left[1 + \frac{\epsilon_{FF}}{\underline{\Phi}_{FF}} + \frac{e^{j\phi_1}}{\underline{H}_T\underline{\Phi}_{FF}}\,\epsilon_{NF} - \frac{e^{j\phi_2}}{\underline{\Phi}_{FF}}\,\epsilon_{PF}\right]}{\left[1 - \frac{\underline{J}}{\underline{\Phi}_{FF}}\,e^{j\phi_1}\,\epsilon_{NF} + \frac{\epsilon_{FF}}{\underline{\Phi}_{FF}} - \frac{e^{j\phi_2}}{\underline{\Phi}_{FF}}\,\epsilon_{PF}\right]} \tag{36}$$

Since we assume that we are dealing with small errors, the following first order approximation may be used to simplify the expression for $\underline{H}$.

$$\frac{1 + \Delta x}{1 + \Delta y} = 1 + \Delta x - \Delta y \tag{37}$$

Rewriting (36) in the light of (37) we have:

$$\underline{H} = \underline{H}_T\left[1 + \frac{\epsilon_{FF}}{\underline{\Phi}_{FF}} + \frac{e^{j\phi_1}\,\epsilon_{NF}}{\underline{H}_T\,\underline{\Phi}_{FF}} - \frac{e^{j\phi_2}\,\epsilon_{FF}}{\underline{\Phi}_{FF}} + \frac{\underline{J}\,e^{j\phi_1}\,\epsilon_{NF}}{\underline{\Phi}_{FF}} - \frac{\epsilon_{FF}}{\underline{\Phi}_{FF}} + \frac{e^{j\phi_2}\,\epsilon_{FF}}{\underline{\Phi}_{FF}}\right] \tag{38}$$

This simplifies by algebraic cancellation so that simulator noise and input signal fluctuations drop out. The significance of this is that $\underline{H}$ is approximately independent of these small error quantities, even though they are part of the perceptual input to the pilot.

$$\underline{H} = \underline{H}_T\left[1 + \left[\frac{1/\underline{H}_T + \underline{J}}{\underline{\Phi}_{FF}}\right] e^{j\phi_1}\,\sigma_{NF}\right] \tag{39}$$

Before continuing we need to know two things: how to combine the real and imaginary parts of the error, and the magnitude of the error standard deviation σ_{NF}. We will first consider the combination of real and imaginary parts. Therefore as an aside consider the following. Let x and y be two real random variables having magnitudes equal to unity and having $\sigma_x = \sigma_y = \Delta$. The true correlation for these variables $\rho_{xy} = \langle xy \rangle = 0$, but $r_{xy} = \overline{xy} = 0 + \epsilon$, where $\bar{\epsilon} = 0$ $\epsilon^2 = \sigma_\epsilon^2$ and where ϵ is real. Then $\sigma_\epsilon = (1/\sqrt{n})$; n being the degrees of freedom in the estimate for ρ_{xy}. (40)

Now consider x and y to be complex numbers distributed on the plane with equiprobable phase. (41)

$$\overline{xy} = \rho_{xy} + \epsilon_1 + j\,\epsilon_2 = 0 + \epsilon_1 + j\,\epsilon_2$$

We can be sure that σ_{ϵ_1} and σ_{ϵ_2} are both proportional to $1/\sqrt{n}$, but it will be necessary to determine the constant of proportionality.

Write $x = a + jb$ and $y = c + jd$. The quantities a, b, c, and d are independent and have equal standard deviations. Compute the expansion for the magnitude of $\overline{XX^*}$ as follows:

$$1 = \overline{(a + jb)(a - jb)} = \overline{a^2} + \overline{b^2} = \overline{\sigma_a^2} + \overline{\sigma_b^2} \qquad (42)$$

$$\therefore \sigma_a = \sigma_b = \sigma_c = \sigma_d = 1/\sqrt{2}$$

Now the expansion for the complex correlation is:

$$\overline{xy} = \overline{(a + jb)(c + jd)} = ac - bd + j(bc - ad) \qquad (43)$$

The above can be evaluated by noting that $\overline{ac}$ is the measured correlation between real independent variables each with standard deviation equal to $1/\sqrt{2}$. Thus in standard form one has

$$r_{ac} = \frac{\overline{ac}}{\sigma_a \sigma_c} = 0 + \epsilon_{ac} \qquad (44)$$

where ϵ_{ac} has a standard deviation of $1/\sqrt{n}$ as in (40). Therefore $\underline{ac}$ has a standard deviation σ_{ac} equal to $1/2\sqrt{n}$. Equation (33) may be re-written as

$$\overline{xy} = \epsilon_1 + \epsilon_2 + j(\epsilon_3 + \epsilon_4) \qquad (45)$$

Each error term in (45) has a standard deviation which equals $1/2\sqrt{n}$. Combining standard deviations for the real and imaginary parts by the square root of the sum of the squares (45) becomes, in the form of (41).

$$\overline{xy} = 0 + \epsilon_1 + j\epsilon_2, \text{ where } \sigma_{\epsilon_1} = \sigma_{\epsilon_2} = \frac{1}{\sqrt{2n}} \qquad (46a)$$

or, alternatively, $\overline{xy} = e^{j\phi}\epsilon_3$; where $\sigma_{\epsilon_3} = \frac{1}{\sqrt{n}}$ and the phase is equi-probable. (46b)

One further argument based on analogies with known relations in the real domain is needed to obtain the magnitude of σ_{NF}. Since we know that $\sigma_{FF} = \bar{\phi}_{FF}/\sqrt{T\Delta f}$, where $T\Delta f = n$, we can reasonably believe that

$$\sigma_{NF} = \frac{\sqrt{\bar{\phi}_{NN}\,\bar{\phi}_{FF}}}{\sqrt{T\Delta f}} \qquad (47)$$

This compares with equation (46b).

Returning to equation (39) and the main line of the argument for obtaining sampling variances, let us separate real and imaginary parts and introduce the results of equation (46) and (47) into (39).

$$\underline{H} = \underline{H}_T \left[1 + \left\{ \frac{\left(\frac{1}{\underline{H}_T} + \underline{J} \right)}{\bar{\Phi}_{FF}} \cdot \frac{\sqrt{\bar{\Phi}_{NN}\, \bar{\Phi}_{FF}}}{\sqrt{T\Delta f}} \right\} \left(\frac{\epsilon_R}{\sqrt{2}} + J \frac{\epsilon_I}{\sqrt{2}} \right) \right] \tag{48}$$

In this expression the ϵ's are random variables for which $\bar{\epsilon} = 0$ and $\overline{\epsilon^2} = 1$, so that $(\epsilon_R + j\, \epsilon_I)$ is distributed circularly on the H plane.

To see how one obtains amplitude and phase standard deviations from (48), rewrite (48) in a simpler form:

$$\underline{H} = \underline{H}_T \left[1 + k_1 + j\, k_2 \right] \tag{49}$$

Assume the error corrections are small, which is reasonable, for otherwise this whole development is meaningless.

Rewriting (49) in different terms

$$\begin{aligned} |\underline{H}|\, e^{j\angle \underline{H}} &= |\underline{H}_T|\, e^{j\angle \underline{H}_T} \left[1 + k_1 + j\, k_2 \right] \\ &\simeq |\underline{H}_T|\, e^{j\angle \underline{H}} \left[1 + k_1 \right] e^{j k_2} \end{aligned} \tag{50}$$

The justification for the approximation in (50) is illustrated in Figure 38.

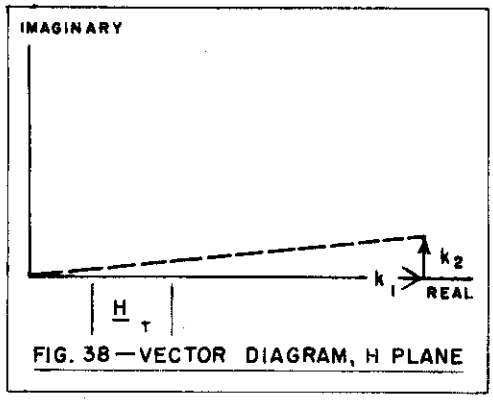

FIG. 38—VECTOR DIAGRAM, H PLANE

The change in the magnitude of the $\underline{H}_T$ vector is negligible except along $\underline{H}_T$; therefore the error in magnitude is simply k_1. Similarly since one can equal real and imaginary parts of (50)

$$\angle \underline{H} = \angle \underline{H}_T + k_2 \tag{51}$$

Accordingly the error in phase is simply k_2.

Going back to equation (48) and using (50) and (51) one can write the following.

For amplitude the sampling standard deviation, $_s\sigma_{amp}$, is:

$$_s\sigma_{amp} = \left|1 + \underline{J}\,\underline{H}_T\right| \sqrt{\frac{\bar{\Phi}_{NN}}{\bar{\Phi}_{FF}}} \frac{1}{\sqrt{2T\Delta f}} \tag{52}$$

and for phase the sampling standard deviation, $_s\sigma_{PH}$, is:

$$_s\sigma_{PH} = \left|\frac{1}{\underline{H}_T} + \underline{J}\right| \sqrt{\frac{\bar{\Phi}_{NN}}{\bar{\Phi}_{FF}}} \frac{1}{\sqrt{2T\Delta f}} \tag{53}$$

Note the influence of "normalized" man generated noise in the above expressions.

Let us now turn to the task of estimating the effects of computational noise. To do this we will write $\underline{H}$ in the form in which it is measured. See Appendix II.

$$\underline{H} = \frac{\bar{C}\bar{F}^*}{\bar{E}\bar{F}^*} = \frac{(Co^+_{CF} - Co^-_{CF}) + j(Qua^+_{CF} - Qua^-_{CF})}{(Co^+_{EF} - Co^-_{EF}) + j(Qua^+_{EF} - Qua^-_{EF})} \tag{54}$$

The following notation will prove convenient

$$Co^+_{CF} = \overline{c + f}$$

$$Co^-_{CF} = \overline{c - f}$$

$$Qua^+_{CF} = \overline{\gamma + \phi}$$

$$Qua^-_{CF} = \overline{\gamma - \phi}$$

and similarly in Roman and Greek lower case letters for E and F.

Equation (54) may now be rewritten as

$$\underline{H} = \frac{\overline{c+f} - \overline{c-f} + j(\overline{\gamma+\phi} - \overline{\gamma-\phi})}{\overline{e+f} - \overline{e-f} + j(\overline{\eta+\phi} - \overline{\eta-\phi})} \tag{55}$$

As in the first part of this appendix, $\underline{H}$ will be expressed as $\underline{H}_T$ plus correction terms. The error terms will be of two kinds; correlated fractional error, β, and uncorrelated fractional error Δ. Thus

$$c+f = \langle c + f\rangle (1 + \beta_1 + \Delta_1) \tag{56}$$
$$c-f = \langle c - f\rangle (1 + \beta_1 + \Delta_2)$$

The correlated errors algebraically cancel so that

$$c+f - c-f = \langle c + f\rangle (1 + \Delta_1) - \langle c - f\rangle (1 + \Delta_2) \tag{57}$$

Equation (55) now becomes

$$\underline{H} = [\langle c + f\rangle - \langle c - f\rangle] + \Delta_1\langle c + f\rangle - \Delta_2\langle c - f\rangle + j[\langle \gamma + \phi\rangle - \langle \gamma - \phi\rangle + \Delta_3\langle \gamma + \phi\rangle - \Delta_4\langle \gamma - \phi\rangle] \tag{58}$$

We will now proceed to define some new variables which will make it easier to convert (58) into the form of $\underline{H}_T$ plus error terms. It will be convenient to have a measure of the difference between Co^+ and Co^- and between Qua^+ and Qua^-. Let us define the quantities α_{ef} and α_{cf} for this purpose.

$$\alpha_{ef} \equiv \frac{\langle e+f\rangle - \langle e-f\rangle + j[\langle \eta+\phi\rangle - \langle \eta-\phi\rangle]}{\sqrt{\langle e+f\rangle^2 + \langle e-f\rangle^2 + j(\langle \eta+\phi\rangle^2 + \langle \eta-\phi\rangle^2)}} \tag{59}$$

α_{cf} is defined analogously. It will also be convenient in the interests of a neater eventual result to define new complex random variables δ_1 for c and f and δ_2 for e and f, in the following manner.

$$\Delta_1\langle c+f\rangle - \Delta_2\langle c-f\rangle + j[\Delta_3\langle \gamma+\phi\rangle - \Delta_4\langle \gamma-\phi\rangle] \equiv \tag{60}$$
$$\delta_1 [\sqrt{\langle c+f\rangle^2 + \langle c-f\rangle^2} + j\sqrt{\langle \gamma+\phi\rangle^2 + \langle \gamma-\phi\rangle^2}] .$$

Now, the variance of the magnitude of δ_1, will be computed in terms of the variance of the fractional error, Δ. Since Δ_1, Δ_2, Δ_3 and Δ_4 have equal variances one can write the following, after taking the square root of the sum of the squares of (60):

$$\sqrt{\sigma_\Delta^2 \langle c+f\rangle^2 + \sigma_\Delta^2 \langle c-f\rangle^2 + \sigma_\Delta^2 \langle \gamma+\phi\rangle^2 + \sigma_\Delta^2 \langle \gamma-\phi\rangle^2} \tag{61}$$
$$= \sigma_\Delta \sqrt{(\sqrt{\langle c+f\rangle^2 + \langle c-f\rangle^2} + j\sqrt{\langle \gamma+\phi\rangle^2 + \langle \gamma-\phi\rangle^2})^2}$$
$$= \sigma_\Delta \left| \sqrt{\langle c+f\rangle^2 + \langle c-f\rangle^2} + j\sqrt{\langle \gamma+\phi\rangle^2 + \langle \gamma-\phi\rangle} \right|$$

By comparing (60) and (61) one can see that

$$\sigma_{|\delta_1|} = \sigma_\Delta \tag{62}$$

The real and imaginary parts of (60) are approximately equal except for the slightly less than unity gain of the phase shifter multiplying the imaginary part. The resulting almost circular distribution makes the assumption of equiprobability for the phase of δ_1 quite reasonable.

Now we are ready to rewrite (58) in terms of the recently defined α_{ef}, α_{cf}, δ_1 and δ_2.

$$\underline{H} = \frac{\langle c+f\rangle - \langle c-f\rangle + j\langle \gamma+\phi\rangle - \langle \gamma-\phi\rangle}{\langle e+f\rangle - \langle e-f\rangle + j\langle \eta+\phi\rangle - \langle \eta-\phi\rangle} \cdot \frac{\left[1 + \frac{\delta_1}{\alpha_{cf}}\right]}{\left[1 + \frac{\delta_2}{\alpha_{ef}}\right]} \tag{63}$$

By the definition of $\underline{H}_T$ and the first order approximation of (37) one gets

$$\underline{H} = \underline{H}_T \left[1 + \frac{\delta_1}{\alpha_{cf}} - \frac{\delta_2}{\alpha_{ef}}\right] \tag{64}$$

In order to go from (64) to a form defining the variance due to computational noise one must rewrite (64) in the form of (38). Thus using the previously defined random variables used in (38) and the results of (42) one has:

$$\underline{H} = \underline{H}_T \left[1 + \frac{\sigma_{|\delta_1|}}{|\alpha_{cf}|\sqrt{2}}(\epsilon_R + j\epsilon_I) + \frac{\sigma_{|\delta_2|}}{|\alpha_{ef}|\sqrt{2}}(\epsilon_R + j\epsilon_I)\right] \tag{65}$$

$$\underline{H} = \underline{H}_T \left[1 + \sqrt{\frac{\sigma^2_{|\delta_1|}}{2\alpha^2_{cf}} + \frac{\sigma^2_{|\delta_2|}}{2\alpha^2_{ef}}}\,(\epsilon_R + j\epsilon_I)\right]$$

By analogy with the reasoning of (52) and (53), the computing noise standard deviations are found to be:

$$CN\sigma_{amp} = \frac{|\underline{H}_T|}{\sqrt{2}} \sqrt{\frac{\sigma^2_{|\delta_1|}}{\alpha^2_{cf}} + \frac{\sigma^2_{|\delta_2|}}{\alpha^2_{ef}}} \tag{66}$$

$$CN\sigma_{PH} = \frac{1}{\sqrt{2}} \sqrt{\frac{\sigma^2_{|\delta_1|}}{\alpha^2_{cf}} + \frac{\sigma^2_{|\delta_2|}}{\alpha^2_{ef}}} \tag{67}$$

The evaluation of (66) and (67) requires an estimate of σ_Δ which equals $\sigma_{|\delta_1|}$. Since σ_Δ is the standard deviation of squared wave analyzer readings, and $[a(1+\Delta)]^2 \simeq a^2[1+2\Delta]$ then $\sigma_{|\delta_1|}$, is twice the standard deviation of the fractional error of the wave analyzer's output.*

* It will be recalled, from equation (56), that σ_Δ may well be considerably smaller than the total wave analyzer error, since systematic errors cancel.

Actually $\sigma_{|\delta_1|}$ has to be estimated higher than σ_Δ since errors occur both in reading the nomograph to determine Co^+, Co^-, Qua^+ and Qua^- as well as in frequency drift of the wave analyzer. Both of these computer errors add variance to the measured cospectra and quadrature spectra.

As to the α's, they must be computed from (59). It will be noted that the α's make for large errors when taking small differences of large numbers.

In order to obtain the total standard deviation in phase and amplitude one must combine the variances for the computer noise and sampling errors. Thus from equations (52) and (66)

$$\sigma_{amp} = \sqrt{{}_s\sigma^2_{amp} + {}_{CN}\sigma^2_{amp}} = \sqrt{\left[|1 + \underline{J}\,\underline{H}_T|\sqrt{\frac{\bar{\Phi}_{NN}}{\bar{\Phi}_{FF}}\frac{1}{\sqrt{2T\Delta f}}}\right]^2 + \left[\frac{|\underline{H}_T|}{\sqrt{2}}\sqrt{\frac{\sigma^2_{|\delta_1|}}{\alpha^2_{cf}} + \frac{\sigma^2_{|\delta_2|}}{\alpha^2_{ef}}}\right]^2} \tag{68}$$

and from (53) and (67)

$$\sigma_{PH} = \sqrt{{}_s\sigma^2_{PH} + {}_{CN}\sigma^2_{PH}} = \sqrt{\left[\left|\frac{1}{\underline{H}_T} + \underline{J}\right|\sqrt{\frac{\bar{\Phi}_{NN}}{\bar{\Phi}_{FF}}\frac{1}{\sqrt{2T\Delta f}}}\right]^2 + \left[\frac{1}{\sqrt{2}}\sqrt{\frac{\sigma^2_{|\delta_1|}}{\alpha^2_{cf}} + \frac{\sigma^2_{|\delta_2|}}{\alpha^2_{ef}}}\right]^2} \tag{69}$$

In equations (68) and (69) the following terms are readily available: T, Δf, and $\bar{\Phi}_{FF}$. The following terms may be either computed easily or else approximated: α_{cf}, α_{ef}, $\sigma_{|\delta|}$, $\underline{J}$, and $|\underline{H}_T| \cong |\underline{H}|$. The one remaining term, $\bar{\Phi}_{NN}$, will be troublesome to evaluate.

$\bar{\Phi}_{NN}$, as it has been defined in this report, is open loop uncorrelated pilot noise. Clearly, direct measurements cannot be made of this quantity. Let us evaluate $\bar{\Phi}_{NN}$ and $\underline{J}$ for the simple case of a direct tracker, as was defined in the body of this report. Under these conditions $\underline{J} = |\underline{J}| = 1$. $\bar{\Phi}_{NN}$ can be evaluated by considering the equations for the Fourier transforms from Figure (5). Thus, since

$$C = \frac{N + \underline{H}\,F}{1 + \underline{H}} \tag{70}$$

$$\bar{\Phi}_{CC} = \frac{1}{|1 + \underline{H}|^2}\left[\bar{\Phi}_{NN} + |\underline{H}|^2\,\bar{\Phi}_{FF}\right] \tag{71}$$

$$\bar{\Phi}_{CF} = \frac{\underline{H}}{1 + \underline{H}}\bar{\Phi}_{FF}$$

Combining (70) and (71) one finds that for a simple tracker:

$$\bar{\Phi}_{NN} = \left[\bar{\Phi}_{CC} - \frac{|\bar{\Phi}_{CF}|^2}{\bar{\Phi}_{FF}}\right] \times [1 + \underline{H}]^2 \tag{72}$$

Equation (72) has the term $(1 + \underline{H})^2$ which converts closed loop noise power to open loop noise power. In other words $(1 + \underline{H})^2$ denotes the reduction the human operator makes in his noise output power because of negative feedback in the visual display.

As regards the airplane simulator, by similar reasoning to that used for (72), one can determine the following expression for the open loop man noise in the simulator

$$\bar{\Phi}_{NN} = \left[\bar{\Phi}_{CC} - \frac{|\bar{\Phi}_{CF}|^2}{\bar{\Phi}_{FF}} \right] |1 + \underline{J}\ \underline{H}|^2 \qquad (73)$$

In the foregoing development $\bar{\Phi}_{FF}$ was assumed to be small.

As to $\underline{J}$; the measurement of this quantity is quite difficult. For the purposes of equations (70) and (71) it will probably suffice if one roughly approximates $\underline{J}$ aileron and $\underline{J}$ elevator as follows:

$$\underline{J} \text{ aileron} \simeq \frac{1}{[j(\omega/\omega_a)]^2\ [1 + j(\omega/\omega_s)]} \qquad (74)$$

and

$$\underline{J} \text{ elevator} \simeq \frac{1}{j(\omega/\omega_e)}$$

The constants have the following values: $\omega_a = 0.58$, $\omega_s = 0.189$, and $\omega_e = 0.18$.

At this point the reader is urged to read references 19 through 23 in the Bibliography.